Neuron
Article

Reelin Regulates Cadherin Function via Dab1/Rap1 to Control Neuronal Migration and Lamination in the Neocortex

Santos J. Franco,[1,2] Isabel Martinez-Garay,[1,2] Cristina Gil-Sanz,[1] Sarah R. Harkins-Perry,[1] and Ulrich Müller[1,*]
[1]Dorris Neuroscience Center and Department of Cell Biology, The Scripps Research Institute, La Jolla, CA 92037, USA
[2]These authors contributed equally to this work
*Correspondence: umueller@scripps.edu
DOI 10.1016/j.neuron.2011.01.003

SUMMARY

Neuronal migration is critical for establishing neocortical cell layers and migration defects can cause neurological and psychiatric diseases. Recent studies show that radially migrating neocortical neurons use glia-dependent and glia-independent modes of migration, but the signaling pathways that control different migration modes and the transitions between them are poorly defined. Here, we show that Dab1, an essential component of the reelin pathway, is required in radially migrating neurons for glia-independent somal translocation, but not for glia-guided locomotion. During migration, Dab1 acts in translocating neurons to stabilize their leading processes in a Rap1-dependent manner. Rap1, in turn, controls cadherin function to regulate somal translocation. Furthermore, cell-autonomous neuronal deficits in somal translocation are sufficient to cause severe neocortical lamination defects. Thus, we define the cellular mechanism of reelin function during radial migration, elucidate the molecular pathway downstream of Dab1 during somal translocation, and establish the importance of glia-independent motility in neocortical development.

INTRODUCTION

In the mammalian neocortex, neurons with similar properties are segregated into specific cell layers that are generated by a series of cell migration events. According to the classical view of neocortical development, projection neurons are born in the ventricular zone (VZ) and migrate along processes of radial glia cells (RGCs) into the developing cortical plate (CP) (Rakic, 1972). However, recent real-time imaging studies demonstrate that radial migration is more complex. After leaving the VZ, newly born neurons adopt a multipolar morphology and migrate through the subventricular zone (SVZ) independently of RGC processes (Tabata and Nakajima, 2003). In the intermediate zone (IZ), migrating neurons assume a bipolar morphology, attach to RGCs, and migrate into the CP by glia-guided locomotion (Noctor et al., 2004). Near the marginal zone (MZ), migrating neurons attach their leading processes to the MZ and switch to glia-independent somal translocation (Nadarajah et al., 2001). During somal translocation, neurons shorten their leading processes to move their cell bodies to their final positions. Importantly, during early stages of neocortical development the CP is sufficiently thin that migrating neurons can extend leading processes to the MZ and migrate by glia-independent somal translocation alone (Morest, 1970; Nadarajah et al., 2001; Shoukimas and Hinds, 1978). Additionally, some neurons inherit the radial processes of their RGC precursors and translocate their cell bodies along these processes to settle in appropriate cell layers (Miyata et al., 2001).

The complex behavior of radially migrating neurons suggests that distinct molecular machineries control each migration step. Consistent with this idea, disruption of different signaling pathways affects cortical lamination in discrete ways. For example, positioning of late-born, but not early-born neurons is defective upon disruption of Cdk5/p35/p39 (Chae et al., 1997; Gilmore et al., 1998; Ko et al., 2001), Dcx (Bai et al., 2003), Lis1 (Tsai et al., 2007), Ndel1 (Shu et al., 2004), and N-cofilin (Bellenchi et al., 2007). In contrast, genetic or chemical perturbation of other signaling pathways such as reelin/Apoer2/Vldlr/Dab1 (Howell et al., 1997; Sheldon et al., 1997; Trommsdorff et al., 1999; Ware et al., 1997), Crk/CrkL/C3G (Park and Curran, 2008; Voss et al., 2008), and PI3K/Akt (Bock et al., 2003; Jossin and Goffinet, 2007) cause defects in superficial and deep layers.

One of the best-known signaling molecules required for neocortical development is reelin. Mutations in the reelin signaling pathway in humans cause lissencephaly and cerebellar hypoplasia (Hong et al., 2000). Mice with mutations in reelin or its receptors or effectors have severe CNS abnormalities, including the inability of migrating deep-layer neurons to split the preplate and of later-born neurons to migrate past earlier-born neurons (Rice and Curran, 2001). Reelin is prominently expressed in the developing neocortex in Cajal-Retzius cells in the MZ (Alcántara et al., 1998; D'Arcangelo et al., 1997; Ogawa et al., 1995) and binds to the Vldlr and Apoer2 receptors (D'Arcangelo et al., 1999; Hiesberger et al., 1999), which are expressed in RGCs and migrating neurons (Luque et al., 2003; Magdaleno et al., 2002; Sheldon et al., 1997; Trommsdorff et al., 1999). The cytoplasmic domains of these receptors bind to the adaptor protein Dab1, which is phosphorylated by Src-family kinases (SFKs) upon reelin binding to its receptors (Arnaud et al., 2003; Howell

et al., 1999). Phosphorylated Dab1 recruits several molecules, including PI3K (Bock et al., 2003), Crk/CrkL (Ballif et al., 2004; Chen et al., 2004; Huang et al., 2004), and Lis1 (Assadi et al., 2003), but the cellular functions that are regulated by these effectors are not well understood. As a result, contrasting models have been proposed for the cellular mechanisms of how reelin controls neocortical development. For example, reelin has been proposed to act as a chemoattractant (Gilmore and Herrup, 2000), repellent (Ogawa et al., 1995; Schiffmann et al., 1997), stop (Sheppard and Pearlman, 1997) or detachment (Dulabon et al., 2000; Sanada et al., 2004; Sheppard and Pearlman, 1997) signal for migrating neurons.

To distinguish between different models of reelin function, we have generated mice carrying floxed *Dab1* alleles. Using timed in utero electroporation of CRE and mice expressing CRE, we show that Dab1 is dispensable for multipolar migration and glia-guided locomotion. Instead, Dab1 regulates somal translocation of early- and late-born neurons by stabilizing their leading processes. Although reelin regulates RGC morphology, we show that a deficit in migrating neurons alone can account for defects in preplate splitting and layer formation caused by absence of reelin. Furthermore, we demonstrate that Dab1 acts via the small GTPase Rap1 to regulate translocation, and that Rap1 in turn controls cadherin function in migrating neurons.

RESULTS

Generation of Dab1-flox Mice

To define the cellular mechanisms by which reelin regulates neocortical development, we generated mice carrying a conditional *Dab1* allele in which loxP sites flank exon 2 (Figures S1A–S1C, available online), which encodes part of the PTB domain that is essential for Dab1 function (Howell et al., 1997). Homozygous $Dab1^{flox/flox}$ mice had normal Dab1 levels in the brain, whereas Dab1 was undetectable in brains from $Dab1^{flox/flox}$ mice crossed to *Nestin-CRE* mice (referred to as *Dab1-NESTINko*) (Figure S1D), which express CRE in neuronal precursors (Graus-Porta et al., 2001). $Dab1^{flox/flox}$ mice had no obvious defects, whereas *Dab1-NESTINko* mice exhibited ataxia and tremors (not shown), characteristic of the *reeler*-like phenotype of *Dab1* null mice.

Dab1 Is Required in Early-Born Neurons for Glia-Independent Somal Translocation

To inactivate *Dab1* in neurons migrating by different modes, we generated an expression vector that uses a fragment of the mouse doublecortin (*Dcx*) promoter (Wang et al., 2007) to drive expression of CRE and EGFP (Dcx-CRE-iGFP) in postmitotic but premigratory neurons (Figures S1E and S1F). Dcx-CRE-iGFP was electroporated in utero into *Dab1-flox* embryos at different ages to analyze effects of *Dab1* inactivation on migration.

Since most early-born neurons are thought to migrate at embryonic day (E) 13–14 by glia-independent somal translocation (Nadarajah et al., 2001), we used in utero electroporation at E12.5 to knock out *Dab1* in these cells (Figure 1A). Five days later, control neurons had migrated into the developing CP (Figure 1B, left panel; control = 92% ± 4% [standard deviation, SD] in CP). In contrast, mutant neurons accumulated below the subplate near the IZ (Figure 1B, right panel; mutant = 4% ± 2% [SD] in CP). When analyzed earlier at E14.5, control and mutant neurons were polarized and had leading processes that extended across the nascent CP (Figure 1C). However, a large number of control neurons, but few mutant neurons, had entered the CP at E14.5 (Figure 1C).

At E15.5, control neurons showed translocating morphologies characterized by leading processes that terminated in the MZ (Figure 1D, top panels). In contrast, mutant neurons displayed multipolar morphologies with stunted processes that no longer extended radially into the CP (Figure 1D, bottom panels). Mutant neurons were rarely found in the CP and remained intermingled with subplate cells. As a consequence, the cortical plate above the electroporated region was reduced in size and the area below the subplate was enlarged due to the accumulation of mutant neurons (Figure 1D). These data demonstrate that Dab1 is not required for initial polarization or process extension of early-born neurons, but is necessary for their migration into the CP, consistent with a cell-autonomous role for Dab1 during splitting of the preplate by deep-layer neurons. As glia-independent somal translocation is the predominant migration mode used by early-born neurons, our data show that Dab1 is necessary for this migration mode.

Dab1 Is Required in Late-Born Neurons for the Terminal Phase of Migration

Neurons destined for upper cortical layers use a sequence of different migration modes: multipolar migration, followed by glia-guided locomotion, and finally terminal somal translocation (Nadarajah et al., 2001; Noctor et al., 2004; Tabata and Nakajima, 2003). To determine the role of Dab1 in these migration modes, we electroporated *Dab1-flox* mice with Dcx-CRE-iGFP at E15.5, when upper-layer neurons are generated (Figure 2A), and analyzed the cells at subsequent ages: E17.5, when wild-type neurons migrate by multipolar migration; P0, when they migrate through the IZ and lower CP along RGC processes and through the upper CP by somal translocation; and P3, when they have reached their final positions. Immunohistochemistry demonstrated that Dab1 protein was absent from electroporated cells by E17.5 (Figure S2), prior to radial migration. This is consistent with our findings that CRE electroporations at E12.5 cause severe phenotypes as early as 2 days later (Figure 1C) and indicates that Dab1 was effectively inactivated.

At E17.5 control and mutant neurons exhibited multipolar morphologies and were located in the multipolar accumulation zone (MAZ) (Tabata et al., 2009) (Figure 2B). At P0, many control and mutant neurons had moved into the upper IZ and lower CP and exhibited bipolar morphologies characteristic of neurons migrating along RGCs (Figure 2C). However, while many control neurons occupied the most superficial layers of the CP, almost none of the mutant neurons had entered the upper layers (Figure 2C). At P3, nearly all control neurons were located in a tight band in layers II-III, while mutant neurons were found primarily below layer IV, near the top of layer V (Figure 2D). Mutant neurons exited the SVZ/IZ, entered the CP, and bypassed deep-layer neurons, indicating that glia-dependent locomotion occurred normally. Analysis at P8 demonstrated that control neurons

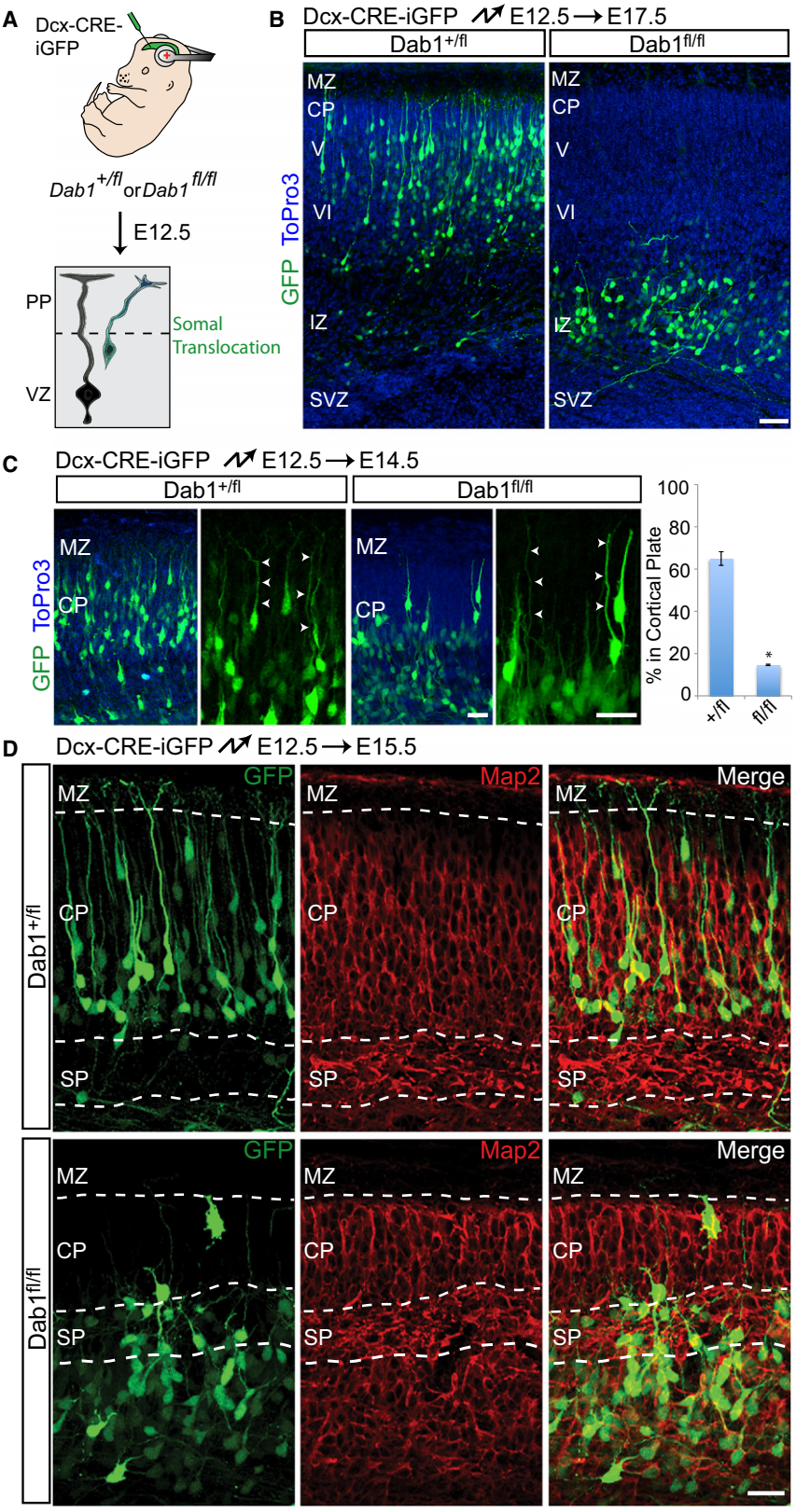

Figure 1. Dab1 Is Required for Glia-Independent Somal Translocation of Early-Born Neurons

(A) Illustration of the strategy to inactivate *Dab1*. Embryos are electroporated in utero with Dcx-CRE-iGFP at E12.5 to target early-born neurons migrating primarily by glia-independent translocation. PP, preplate; VZ, ventricular zone.

(B) Positioning defects of early-born *Dab1*-deficient neurons. Coronal sections from heterozygous (left panel) and homozygous (right panel) *Dab1*^{fl} embryos electroporated at E12.5 and analyzed at E17.5. Electroporated neurons are in green, nuclei in blue.

(C) Correct polarization and process extension by Dab1-deficient neurons. Coronal sections from heterozygous (left panels) and homozygous (right panels) *Dab1*^{fl} embryos electroporated at E12.5 and analyzed at E14.5. Electroporated neurons are in green, nuclei in blue. Arrowheads identify leading processes. Quantification is % of electroporated cells in the CP, ± SEM. *$p < 0.0001$ by Student's t test.

(D) Morphological defects of *Dab1*-deficient neurons. Coronal sections from heterozygous (top panels) and homozygous (bottom panels) *Dab1*^{fl} embryos electroporated at E12.5 and analyzed at E15.5. Migrating electroporated neurons are in green. Immunostaining for Map2 (red) identifies the borders of the CP and SP. CP, cortical plate; IZ, intermediate zone; MZ, marginal zone; SP, subplate; SVZ, subventricular zone. V, layer V; VI, layer VI.

Scale bars: 50 μm (B) and 25 μm (C and D). See also Figure S1.

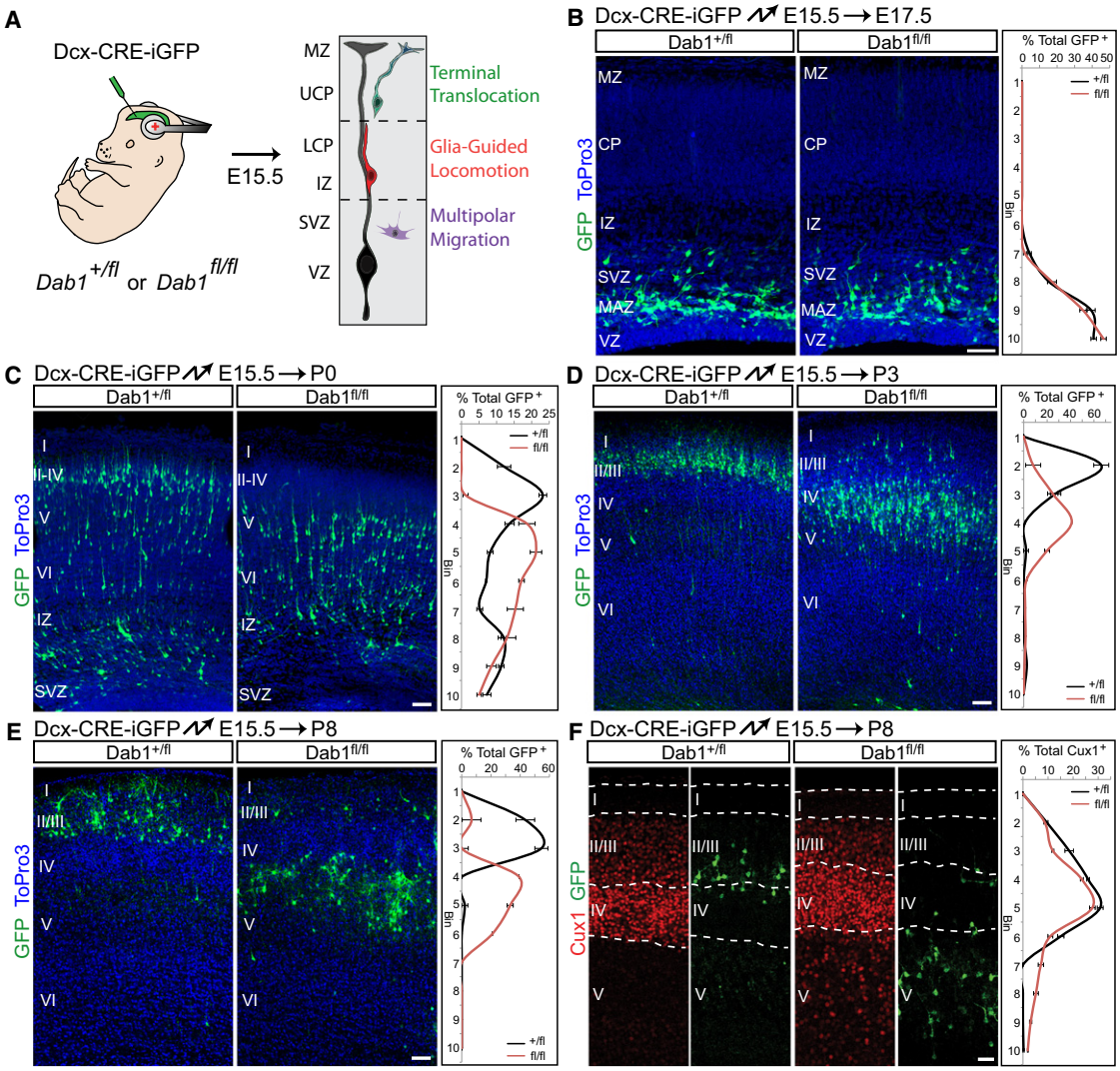

Figure 2. Dab1 Is Required for Migration of Late-Born Neurons into Upper Layers

(A) Illustration of the strategy to inactivate *Dab1*. Embryos are electroporated in utero with Dcx-CRE-iGFP at E15.5 to target late-born neurons that migrate first by multipolar migration, then by glia-guided locomotion and finally terminal translocation. Radial glia cells are shown in black and neurons are colored according to migration modes. MZ, marginal zone; UCP, upper cortical plate; LCP, lower cortical plate; IZ, intermediate zone; SVZ, subventricular zone; VZ, ventricular zone.

(B–E) Defective translocation in late-born *Dab1*-deficient neurons. Coronal sections from heterozygous (left panels) and homozygous (right panels) *Dab1*^{fl} embryos electroporated at E15.5 and analyzed at E17.5 (B), P0 (C), P3 (D), or P8 (E). Electroporated neurons are in green, nuclei in blue. Quantification of cell positions shown at right. Graphs represent positive cells in each of ten equal-size vertical bins expressed as % of total electroporated cells, ± SEM.

(F) Cell-autonomous displacement of mutant upper layer neurons. Coronal sections from E15.5 electroporations performed as in (E) and analyzed at P8. Immunostaining for Cux1 (red) reveals upper-layer neurons located ectopically in deep layers after *Dab1* deletion.

Abbreviations as in Figure 1. Cortical layers are labeled I-VI. Scale bars: 50 μm. See also Figure S2.

occupied layers II/III as expected, while mutant neurons accumulated below layer IV neurons, but above layers V-VI (Figures 2E and 2F). A population of cells expressing the upper layer neuron marker Cux1 was found below layer IV in the mutant, but not control electroporations, indicating that mutant neurons in layer V were misplaced upper-layer neurons (Figure 2F). Mutant neurons therefore bypass their predecessors by glia-guided locomotion, but are unable to complete the final phase of migration to move past neurons that migrated immediately prior to them.

Dab1 Is Not Essential for Glia-Guided Locomotion

To further test the hypothesis that Dab1 is not required for glia-guided locomotion, we performed immunohistochemistry for RGC markers in brains electroporated with Dcx-CRE-iGFP at E15.5 and sectioned at E18.5 (Figure S3A). In control and Dab1 mutant brains, EGFP-positive neurons with the characteristic bipolar morphology of locomoting neurons were readily observed in association with RGC processes in the IZ and CP (Figure S3A), indicating that interactions between neurons and glia were preserved without Dab1.

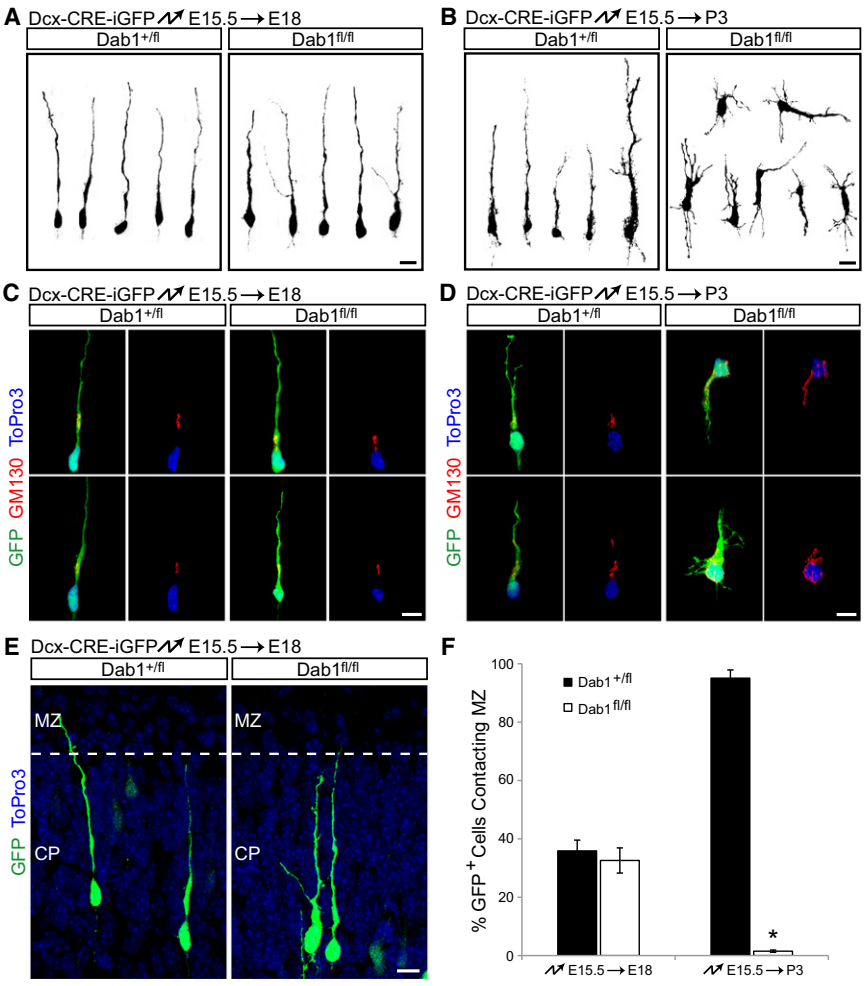

Figure 3. Morphology and Polarity of Migrating Dab1-Deficient Neurons Is Normal at Early Stages but Defective during the Final Phase of Migration

(A and B) Morphological analysis of migrating neurons. Dcx-CRE-iGFP was electroporated into heterozygous (left panels) or homozygous (right panels) *Dab1*^{fl} embryos at E15.5, followed by 3D reconstruction of GFP-positive neurons at E18.5 (A) or P3 (B).

(C and D) Immunohistochemical analysis of polarity of migrating neurons. Electroporations at E15.5 as in (A) and (B), followed by nuclear staining (ToPro3, blue) and immunostaining for the Golgi marker GM130 (red) at E18.5 (C) or P3 (D).

(E) Control and Dab1-deficient neurons initially make contact with the MZ. Electroporations at E15.5 as in (A) and (B), followed by analysis at E18.5. Electroporated neurons are shown in green. ToPro3 stain reveals the borders between the CP and MZ.

(F) Dab1-deficient neurons fail to maintain contact with the MZ. Quantification of the % of electroporated neurons contacting the MZ 3 days (E18.5) and 7 days (P3) after electroporation.

The data represent mean ± SEM. *$p < 0.001$ by Student's t test. Scale bars: 10 μm. See also Figure S3 and Movies S1–S4.

To evaluate glia-guided locomotion directly, we performed time-lapse microscopy (Figures S3B–S3D, Movies S1–S4). As reported (Nadarajah et al., 2001), control neurons migrated in a saltatory pattern, extending leading processes followed by cell body translocation (Figure S3B and S3C, Movies S1 and S2). The behavior of mutant neurons was indistinguishable from controls (Figures S3B and S3C, Movies S3 and S4); no difference in migration speed was observed (control = 10.1 ± 3.2 [SD] μm/hr, mutant = 9.5 ± 2.6 [SD] μm/hr; $p = 0.39$ by t test) (Figure S3D). We conclude that Dab1 is not essential for glia-guided locomotion.

Dab1 Is Required for Stabilization of the Leading Process during Terminal Somal Translocation

As Dab1 is required in early-born neurons for glia-independent somal translocation (Figure 1), we reasoned that Dab1 in late-migrating neurons might similarly affect terminal somal translocation. We therefore analyzed cell morphology of Dab1-deficient neurons at late stages of migration. As outlined above, the morphologies of mutant and control cells electroporated at E15.5 and analyzed prior to somal translocation at E18.5 both exhibited the bipolar shape characteristic of locomoting neurons (Figures 3A and 3C). Staining for pericentrin (not shown) and GM130 (Figure 3C) demonstrated that the centrosome and Golgi apparatus localized ahead of the nucleus in control and mutant neurons, indicative of normal cell polarity. Control and mutant neurons near the top of the CP at E18.5 also had leading processes that contacted the MZ (Figures 3E and 3F). However, at P3, control neurons remained bipolar (Figures 3B and 3D, left panel), while mutant cells showed multipolar morphologies (Figures 3B and 3D, right panel) and oblique or inverted orientations, reminiscent of inverted pyramidal cells characteristic of the *reeler* phenotype (Landrieu and Goffinet, 1981). Polarization of the Golgi apparatus was disrupted in mutant neurons (Figure 3D) and their leading processes no longer contacted the MZ (Figure 3F). This sequence of morphological changes suggests that Dab1-deficient neurons begin to display defects when terminal somal translocation usually occurs.

To test directly whether Dab1 is required for terminal somal translocation, we carried out time-lapse experiments. *Dab1-flox* embryos were electroporated with Dcx-CRE-iGFP at E15.5 and neurons whose leading processes were approaching, but not yet contacting the MZ were analyzed at E18.5. As reported (Nadarajah et al., 2001), control neurons had leading processes of relatively constant lengths until the leading edge contacted the MZ, at which point their leading processes shortened as their cell bodies translocated toward the MZ (Figure 4A, top panels; Movies S5 and S6). Mutant neurons contacted the

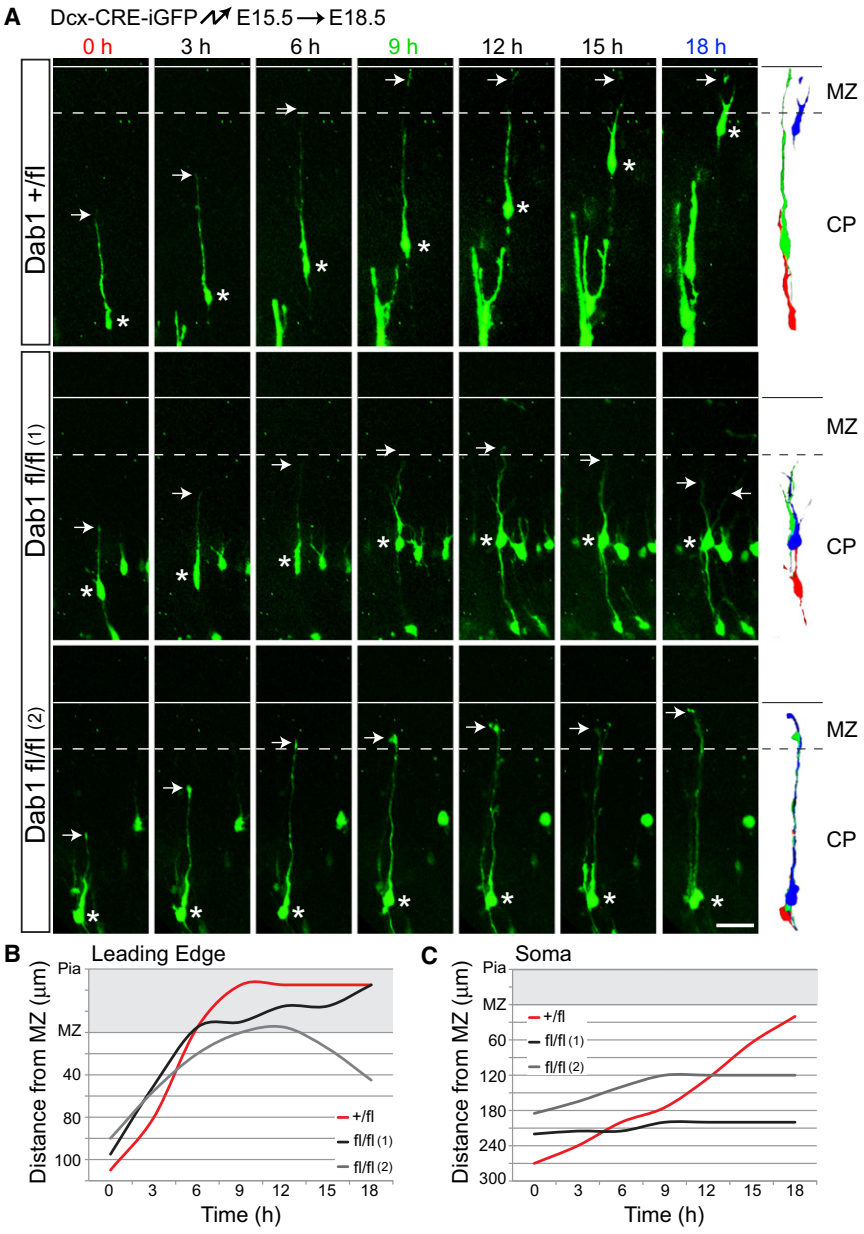

Figure 4. Dab1-Deficient Neurons Fail to Undergo Terminal Somal Translocation

(A) Images from time-lapse experiments tracking electroporated neurons. *Dab1*$^{+/fl}$ and *Dab1*$^{fl/fl}$ embryos were electroporated with Dcx-CRE-iGFP at E15.5 and processed for slice cultures at E18.5. Migrating neurons approaching the MZ were imaged. Top panels show a control (*Dab1*$^{+/fl}$) neuron undergoing terminal translocation over an 18 hr period. Middle panels demonstrate a mutant (*Dab1*$^{fl/fl}$ [1]) neuron failing to complete terminal translocation and instead retracting the leading process (at t = 15 hr) and extending new processes (at t = 18 hr). Bottom panels show a mutant (*Dab1*$^{fl/fl}$ [2]) neuron that does not undergo terminal translocation, but whose leading process remains in the MZ. Arrows identify the leading processes and asterisks label the somas of the sampled neurons. To the right, traces represent migrating neurons at 0 hr (red), 9 hr (green) and 18 hr (blue).

(B and C) Distances from the MZ to the leading edge (B) or cell soma (C) of sampled neurons from (A) are plotted for each time point. The space occupied by the MZ is shaded gray.

CP, cortical plate; MZ, marginal zone. Scale bar: 50 μm. See also Movies S5–S8.

MZ with comparable frequency and at similar time points (Figure 3F), but were almost never observed to undergo terminal translocation. Instead, they retracted their leading processes and began to extend multiple processes (Figure 4A, middle panels; Movies S7 and S8). Some Dab1-deficient neurons retained contact with the MZ for the duration of the experiment, but failed to translocate the cell soma (Figure 4A, bottom panels). Plotting the distance of the leading edge (Figure 4B) or the cell soma (Figure 4C) from the MZ further illustrated the differences in migratory behavior between controls and mutants. We conclude that late-born mutant neurons fail to undergo terminal somal translocation and instead retract their leading processes, lose polarity, and differentiate short of their proper positions.

Rap1 Is Required for Glia-Independent Somal Translocation

Reelin binding to its receptors triggers Dab1 phosphorylation followed by recruitment of PI3K and Crk/CrkL and the activation of their downstream effectors Limk1, Akt1, and Rap1 (Figure 5A); Limk1 regulates F-actin stability in leading neuronal processes while Akt and Rap1 regulate neuronal adhesive properties (Ballif et al., 2004; Bock et al., 2003; Chai et al., 2009; Chen et al., 2004; Huang et al., 2004). To determine the extent to which any of these signaling molecules might mediate Dab1 function during somal translocation, we inactivated them by in utero electroporation at E12.5 (Figure 5B), when cortical neurons migrate predominantly by glia-independent somal translocation. To achieve specific inactivation in migrating neurons without affecting RGCs, we used a Dcx promoter construct that is active in migrating neurons, but not in RGCs (Figure 5B; Figures S1E and S1F) (Wang et al., 2007). Positions of the migrating neurons were determined at E16.5 (Figures 5C–5E). No defects in migration were observed upon expression of dominant-negative Limk1 (Edwards and Gill, 1999) (DN-Limk1; Figures 5B, 5C, and 5E). Limk1 regulates actin cytoskeletal dynamics by phosphorylating N-cofilin, thereby inhibiting its F-actin severing activity (Arber et al., 1998; Yang et al., 1998). We therefore also electroporated constitutive-active N-cofilin (Nagaoka et al., 1996), but again observed no effect on migration

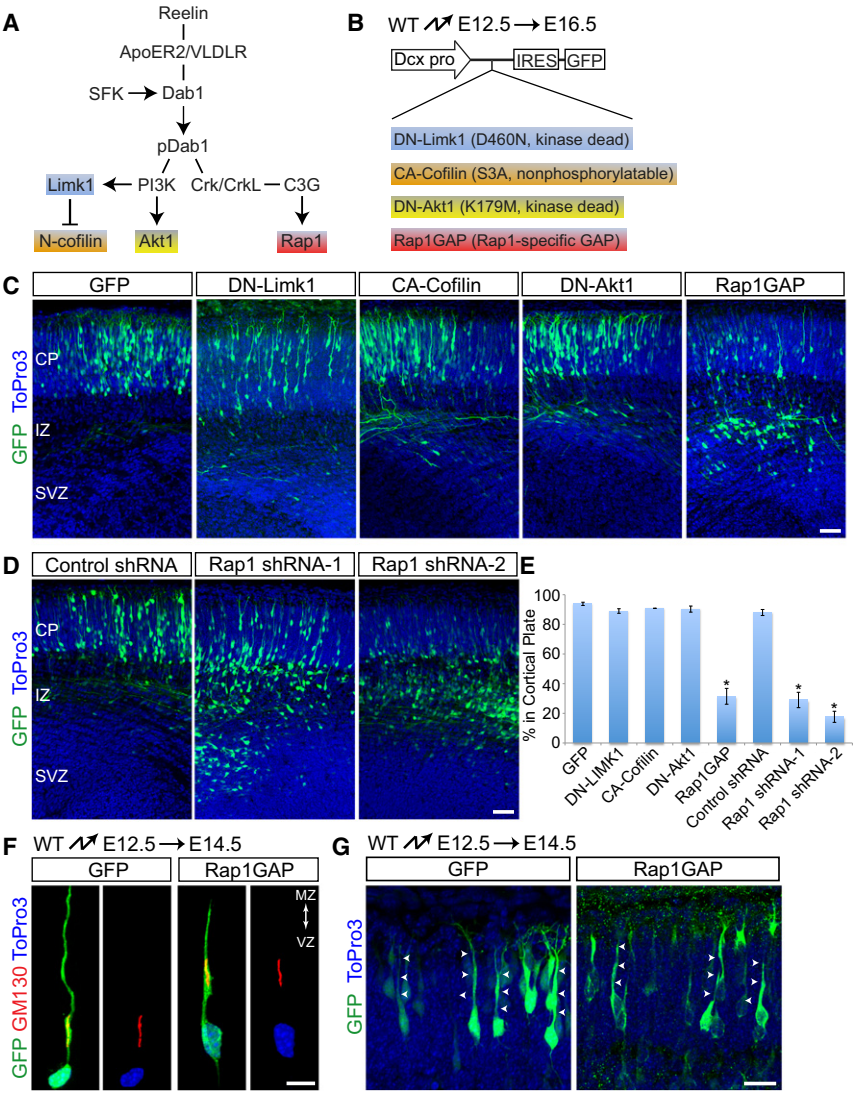

Figure 5. Rap1 Is Required for Glia-Independent Translocation

(A) Illustration of signaling pathways downstream of reelin. Molecules highlighted in different colors represent effectors targeted in (C).

(B) Experimental design for manipulating downstream effectors during glia-independent translocation. Mutant forms of the downstream effectors depicted in (A) were expressed from the Dcx-IRES-GFP vector by in utero elecroporation.

(C and D) Perturbing Rap1, but not other reelin downstream effectors, disrupts glia-independent translocation. (C) Coronal sections from embryos electroporated with the indicated constructs at E12.5 and analyzed at E16.5. Electroporated neurons are shown in green, nuclei in blue. (D) Coronal sections from embryos electroporated at E12.5 with GFP and either nonsilencing control or shRNA constructs targeting Rap1a. Analysis performed at E16.5.

(E) Quantification of % neurons from (C) and (D) that entered the cortical plate. The data represent mean ± SEM. *$p < 0.0001$ by Student's t test.

(F and G) Rap1GAP does not affect initial polarization or process extension. (F) Polarity of neurons electroporated at E12.5 and analyzed at E14.5. Internal polarity is shown by immunostaining for the Golgi marker GM130 (red) and nuclear staining with ToPro3 (blue). (G) Morphological analysis of neurons electroporated as in (F). Arrows point to polarized processes extending to the cortical plate.

Abbreviations as in Figure 1. Scale bars: 50 μm (C and D) and 20 μm (F and G). See also Figure S4.

(CA-Cofilin; Figures 5B, 5C, and 5E). Radial migration of cortical neurons was also not affected by expression of dominant-negative Akt1 (Franke et al., 1995) (DN-Akt1; Figures 5B, 5C, and 5E). However, radial migration was inhibited by expression of a Rap1-specific GAP (Rap1GAP) that reduces Rap1 activity (Han et al., 2006; Rubinfeld et al., 1992) (Figures 5B, 5C, and 5E). Inactivation of Rap1 using small hairpin (sh) RNA constructs that specifically knock down Rap1a expression (Figure S4) also effectively inhibited radial migration (Figures 5D and 5E).

Dab1-deficient neurons initially polarize appropriately but subsequently withdraw their leading processes from the cortical MZ (Figure 1). We therefore anticipated that Rap1-inactivated neurons would also initially polarize but fail to maintain their leading processes, thereby preventing cell body translocation. To test this model, we carried out in utero electroporations at E12.5 and analyzed cell morphology at E14.5. Similar to Dab1-deficient neurons, Rap1GAP-expressing neurons were polarized (Figure 5F) and had leading processes that extended across the nascent CP (Figure 5G). We conclude that Rap1 is not required for the initial polarization or process extension of early-born neurons, but for leading process maintenance and the subsequent translocation of neuronal cell bodies into the CP.

Cadherins Act Downstream of Rap1 to Control Glia-Independent Somal Translocation

Rap1 controls cell adhesion by regulating two prominent classes of adhesion receptors: integrins and cadherins (Kooistra et al., 2007). We hypothesized that Rap1 might affect migration by regulating adhesion molecules to control leading process extension and/or anchorage. Our previous studies have shown that integrins are required for anchorage of glial endfeet at the cortical MZ, but not for neuronal process extension or migration (Belvindrah et al., 2007; Graus-Porta et al., 2001). We therefore focused on cadherins. Immunolocalization studies with an antibody to the cytoplasmic domain of classical cadherins demonstrated their widespread expression in the developing cortical wall (Figure 6A). Interestingly, cadherin expression was substantially higher in the cortical MZ, where the processes of neurons

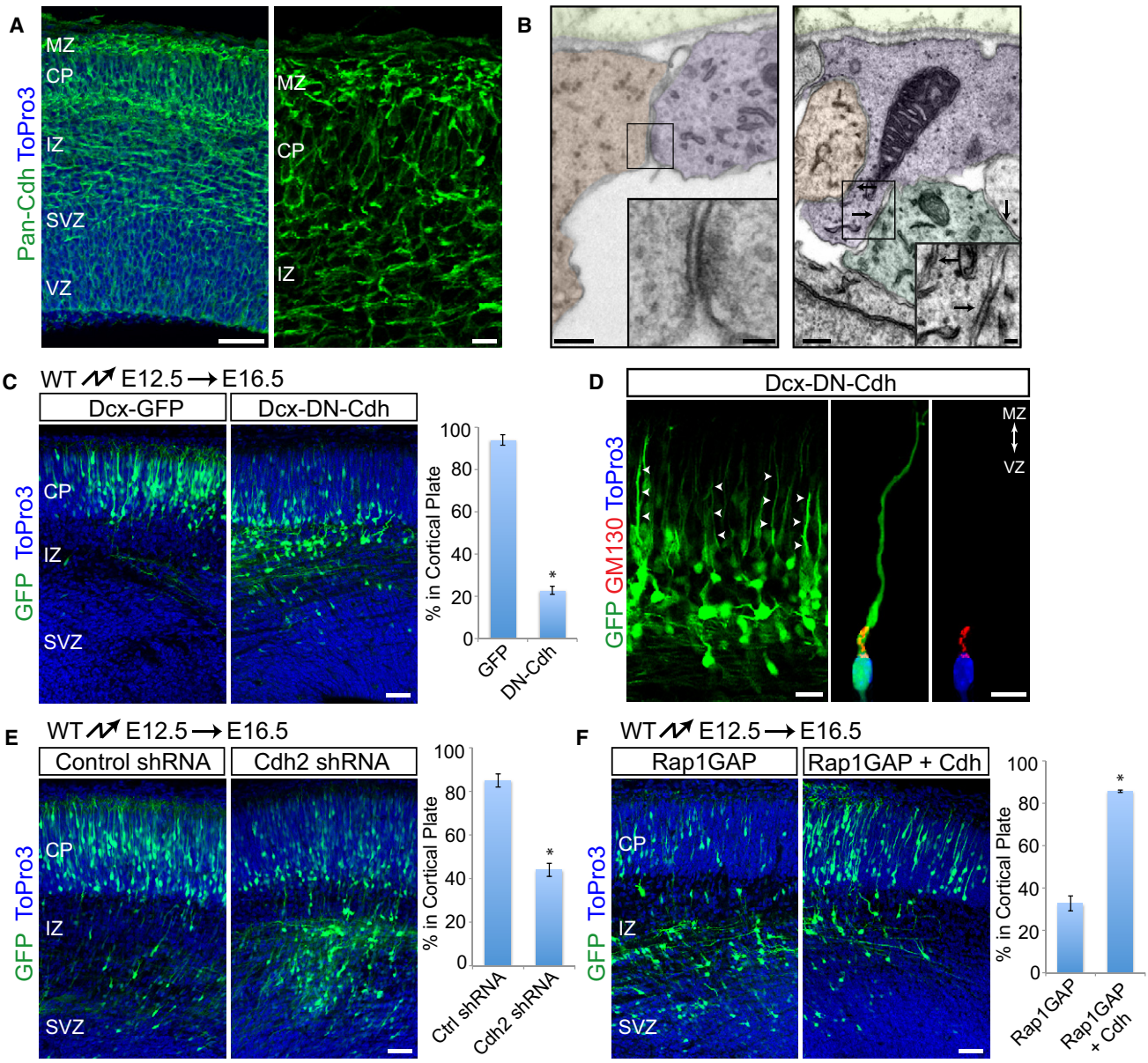

Figure 6. Cadherins Are Required Downstream of Rap1 for Glia-Independent Translocation

(A) Immunostaining with a pan-Cdh antibody shows cadherin expression throughout the cortex at E15.5.

(B) Adherens-junction-like structures in the E15.5 marginal zone. Electron micrographs of coronal sections. Different cell types were distinguished by cytoskeletal specializations and are shaded in different colors (neuronal processes, blue; RGC endfeet, orange, other cells, green). Arrows point to junctional structures.

(C) Positioning defects of neurons expressing dominant-negative cadherin. Coronal sections from embryos electroporated at E12.5 and analyzed at E16.5. Electroporated neurons are shown in green, nuclei in blue. Quantification of % neurons reaching the CP shown at right. The data represent mean ± SEM. *$p < 0.0001$ by Student's t test.

(D) Morphological analysis of neurons electroporated as in (C). Arrows point to processes extending to the cortical plate. Internal polarity is shown by immunostaining for the Golgi marker GM130 (red) and nuclear staining with ToPro3 (blue).

(E) Coronal sections from embryos electroporated at E12.5 with nonsilencing control or an shRNA construct targeting Cdh2. Analysis performed at E16.5. Quantification of % neurons reaching the CP shown at right. The data represent mean ± SEM. *$p < 0.001$ by Student's t test.

(F) Cdh2 overexpression rescues the migration defects of Rap1GAP-electroporated neurons. Coronal sections from E12.5 electroporations with Rap1GAP alone or together with Cdh2, and analyzed at E16.5. Electroporated neurons are green, nuclei blue. Quantification of % neurons reaching the CP is shown at right. The data represent mean ± SEM from three separate experiments. *$p < 0.0001$ by Student's t test.

Abbreviations as in Figure 1. Scale bars: 10 μm (A, right panel, and D, right panel), 20 μm (D, left panel), 50 μm (A, left panel), (B, insets, C, and E), 200 μm (B). See also Figure S5.

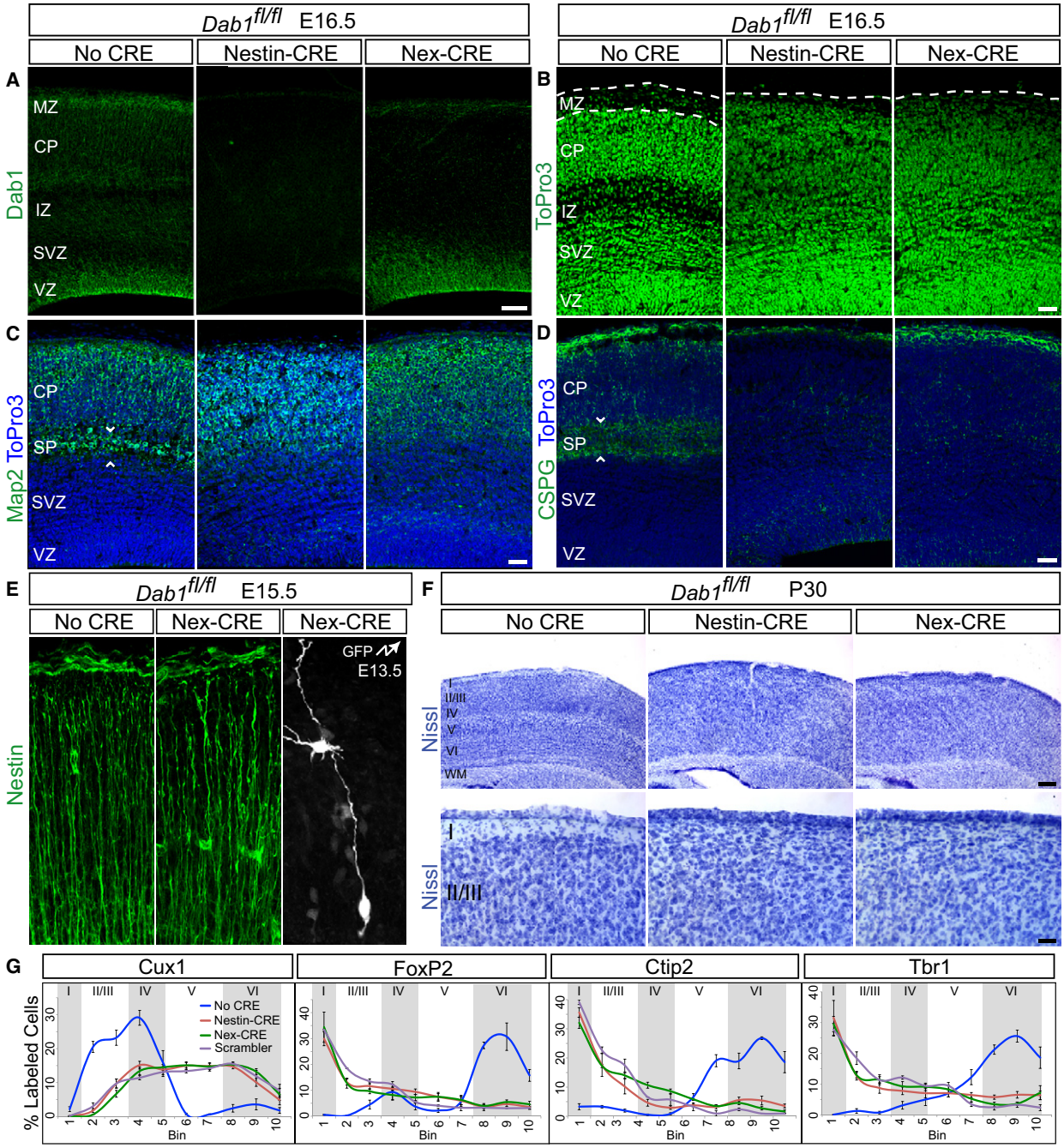

Figure 7. Similar Neocortical Lamination Defects in *Dab1-NESTINko* and *Dab1-NEXko* Mice

(A) Immunostaining for Dab1 at E16.5 shows that Dab1 is expressed throughout the cortical wall in *Dab1*$^{fl/fl}$ (No CRE) embryos, but is lost throughout the cortex in *Dab1-NESTINko* and specifically from neurons in *Dab1-NEXko* embryos. Note Dab1 immunoreactivity in RGCs in the VZ in *Dab1-NEXko*.

(B) ToPro3 nuclear stain at E16.5 demonstrates disrupted cytoarchitecture in *Dab1* mutant embryos compared to control. Dotted lines identify the borders between the pia and CP.

(C and D) Failure to split the preplate in Dab1 mutants. Immunostaining for Map2 (C) and CSPG (D) at E16.5 reveals the SP in control embryos and its absence in mutants. Sections are counterstained with ToPro3 (blue). White arrowheads frame the SP.

(E) Normal RGC morphology in *Dab1-NEXko* mice. Immunostaining for Nestin in control (left panel) and *Dab1-NEXko* (middle panel) cortex at E15.5 demonstrates normal radial morphology of RGC processes. Electroporation of *Dab1-NEXko* cortex with GFP at E13.5 and analysis at E15.5 (right panel) shows a stereotypical RGC spanning the entire cortical wall, anchored at the ventricular and pial surfaces.

(F) Disrupted lamination in adult mutants. Top panels: Nissl-stained neocortex from control and mutant mice at P30. Bottom panels: higher magnification images demonstrating loss of layer I in mutants.

migrating by glia-independent somal translocation are anchored (Figure 6A). Using electron microscopy, we also observed adherens junctions between neuronal processes and other cells in the cortical MZ (Figure 6B). To perturb cadherin function during migration, we expressed a dominant-negative cadherin construct by in utero electroporation at E12.5 and analyzed cell positions at E16.5. At this time point, neurons migrate predominantly by glia-independent somal translocation (Nadarajah et al., 2001), allowing us to study cadherin function in this process without confounding effects from their potential role in glia-dependent motility (Kawauchi et al., 2010). Furthermore, as cadherins and their effector β-catenin control RGC proliferation (Chenn and Walsh, 2002; Machon et al., 2003; Mutch et al., 2010; Woodhead et al., 2006; Zhang et al., 2010), we specifically expressed the dominant-negative cadherin construct in migrating neurons by using the Dcx promoter (Figure S1E) (Wang et al., 2007). Migration of neurons into the CP was severely affected by expression of Dcx-DN-cadherin (Figure 6C). Similar to what we observed for cells deficient for Dab1 or Rap1, cell polarization and extension of leading processes was initially unaffected (Figure 6D), but the processes were subsequently withdrawn (Figure 6C). To exclude that the dominant-negative cadherin affected proliferation or differentiation, we stained the cells with markers for proliferation (Ki67), intermediate progenitor cells (Tbr2), immature neurons (Tuj1), and mature neurons (MAP2) (Figure S5A). The cells were $Tuj1^{+}$/$Ki67^{-}$/$Tbr2^{-}$/$MAP2^{-}$, indicating that they were immature neurons. We conclude that cadherins are required cell-autonomously for stabilizing leading processes during glia-independent somal translocation.

To independently confirm our findings, we perturbed cadherin function by using RNA interference. In agreement with published reports (Kadowaki et al., 2007; Kawauchi et al., 2010), we observed that Cdh2 is prominently expressed throughout the developing cortex (data not shown). We therefore expressed Cdh2-specific shRNAs by in utero electroporation at E12.5 and analyzed cell positions at E16.5. Two Cdh2-specific shRNAs that knocked down its expression (Figure S5B), but not a control nonsilencing shRNA (Figure S5B), effectively inhibited migration (Figure 6E; Figure S5C). The effect was less pronounced than observed with the dominant negative construct, which could be a consequence of incomplete gene silencing. Alternatively, Cdh2 might cooperate with other classical cadherins to control migration.

Previous studies have shown that Rap1 regulates VE- and E-cadherin mediated adhesion (Kooistra et al., 2007). We therefore reasoned that Rap1 might be upstream of cadherin function in migrating neurons. To test this model, we coelectroporated Rap1GAP together with an expression vector for neuronal cadherin (Cdh2). The inhibitory effect of Rap1GAP on radial migration was nearly completely rescued by Cdh2 overexpression (Figure 6F). Taken together, our data suggest that the Dab1 effector Rap1 regulates adhesion and maintenance of the leading processes of migrating neurons as a prerequisite for glia-independent somal translocation. Interestingly, we were unable to rescue the Dab1 null migration phenotype by overexpressing Cdh2 (not shown), suggesting that Rap1-dependent cadherin-mediated adhesion might not be the only mechanism acting downstream of Dab1. Notably, another important aspect of glia-independent somal translocation is nucleokinesis, which is controlled by Lis1 (Tsai et al., 2007). Dab1 binds Lis1 (Assadi et al., 2003), suggesting that Dab1 is required to integrate several aspects of glia-independent somal translocation. It is therefore not surprising that overexpression of Cdh2 rescues Rap1-dependent aspects of Dab1 function, but not other parallel signaling pathways.

Deletion of Dab1 in Migrating Neurons Alone Leads to a *reeler*-like Phenotype

The complexity of abnormalities in *reeler* mice raises the possibility that defects in nonneuronal cells contribute to mispositioning of neurons. For example, reelin is required for maturation of the RGC scaffold (Hartfuss et al., 2003; Hunter-Schaedle, 1997), and defects in RGCs may affect migration (Luque et al., 2003; Miyata et al., 2001). To test this hypothesis, we crossed *Dab1-flox* mice to the *Nex-CRE* line, which expresses CRE in intermediate progenitor cells (IPCs) and migrating neurons, but not in RGCs (Belvindrah et al., 2007; Goebbels et al., 2006). Comparison of $Dab1^{flox/flox}$;*Nex-CRE* mice (referred to as *Dab1-NEXko*) to *Dab1-NESTINko* mice allowed us to determine the neuron-specific contributions to lamination defects.

Immunohistochemistry at E16.5 demonstrated the loss of Dab1 protein from all cells in the *Dab1-NESTINko* neocortex (Figure 7A). In *Dab1-NEXko* mice, the Dab1 signal remained in RGCs, but was lost in IPCs and neurons (Figure 7A). RGC morphology was unaffected in *Dab1-NEXko* mice (Figure 7E), but both *Dab1-NESTINko* and *Dab1-NEXko* mice exhibited loss of the MZ (Figure 7B) and absence of a subplate (Figures 7C and 7D) caused by failure to split the preplate. These phenotypes were identical to those in other Dab1 mutants (Herrick and Cooper, 2002; Howell et al., 1997, 2000; Rice et al., 1998; Sheldon et al., 1997). Nissl staining at subsequent ages also revealed a complete absence of identifiable layers in both mutant strains, including loss of layer I and lack of barrel fields in layer IV (Figure 7F). Immunohistochemistry for layer-specific markers revealed identical neuronal positioning defects in *Dab1-NESTINko*, *Dab1-NEXko* mice and Dab1 null *Scrambler* mice (Figure 7G; Figure S6). Cux1-positive neurons labeled layers II-IV in $Dab1^{flox/flox}$ mice, but were located throughout the lower half of the neocortex in both mutants (Figure 7G; Figure S6A). FoxP2 labeled layers IV and VI in controls, but was expanded throughout the cortical thickness in *Dab1-NESTINko* and *Dab1-NEXko* mice (Figure 7G; Figure S6B). Neurons positive for Ctip2 or Tbr1 were found in deep layers in controls, but more superficially in *Dab1-NESTINko* and *Dab1-NEXko* mice (Figure 7G; Figures S6C and S6D). Thus, lamination defects were indistinguishable between *Dab1-NESTINko* and *Dab1-NEXko* mice, indicating that Dab1-deficiency in migrating neurons is largely responsible for the layering defects.

(G) Quantification of the indicated layer markers at P30. Graphs represent positive cells in each of ten equal-size vertical bins expressed as % total positive cells, ± SEM. Approximate positions of cortical layers are identified by alternating gray and white shaded areas.
Scale bars: 50 μm (A–D), 250 μm (E, top), 50 μm (E, bottom). Neocortical layers are labeled I-VI. WM, white matter. See also Figure S6.

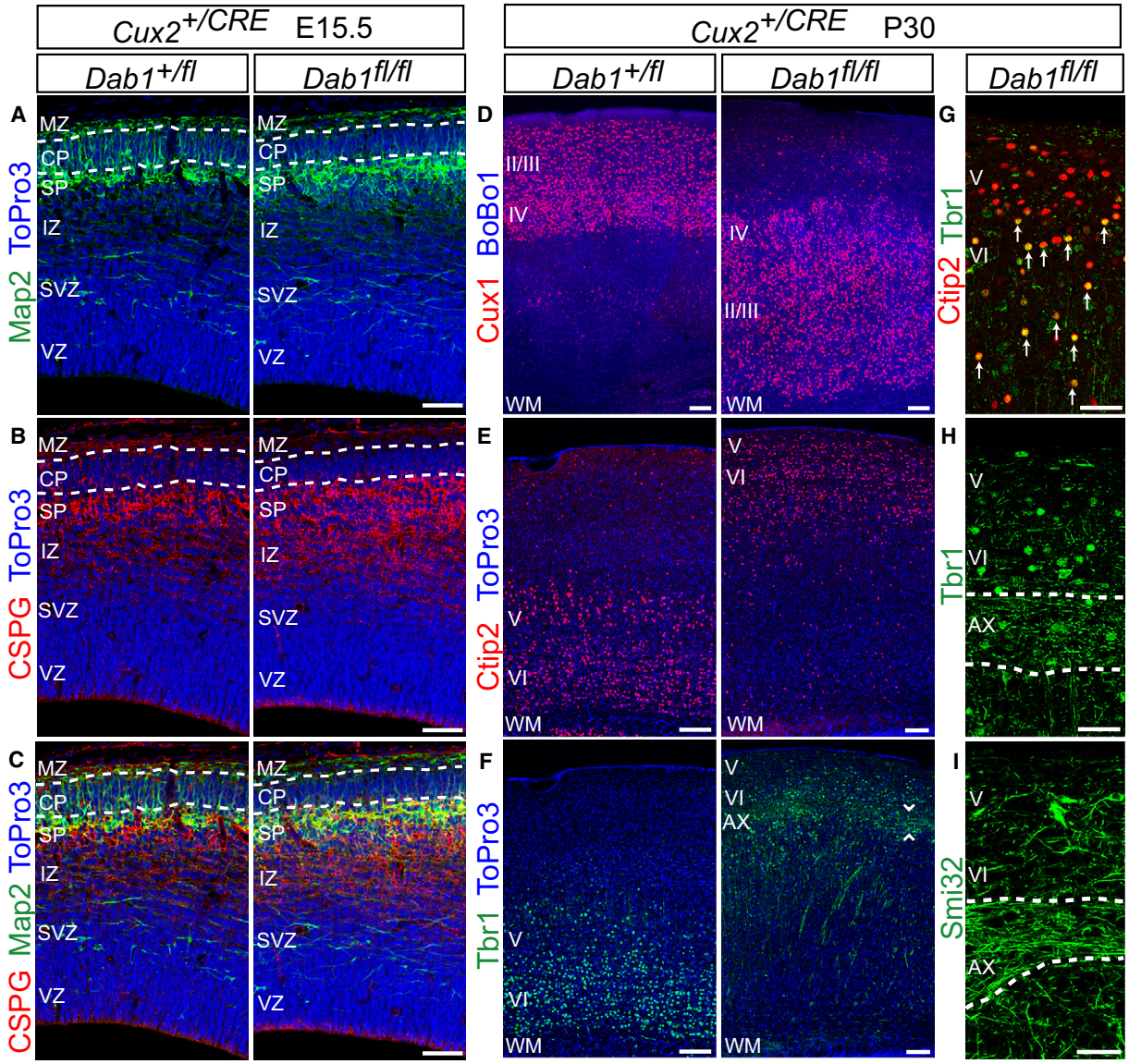

Figure 8. Normal Preplate Splitting but Disrupted Neocortical Lamination in *Dab1-CUX2ko* Mice

(A–C) The preplate is split in *Dab1-CUX2ko* embryos. Immunostaining at E15.5 for Map2 (A) and CSPG (B) reveals the subplate region below the developing CP in control (*Dab1*$^{+/fl}$) and *Dab1-CUX2ko* mutant (*Dab1*$^{fl/fl}$) embryos. Nuclei are in blue. Dotted lines identify the borders between the MZ and CP (upper), and between the CP and SP (lower). (C) Merged images from (A) and (B).

(D–I) Immunostaining for layer markers in P30 control and *Dab1-CUX2ko* mice demonstrates that deep layers form normally, but superficial layers are misplaced in mutants. (D) Immunostaining for Cux1 shows upper-layer neurons misplaced beneath deep-layer neurons in mutants. Sections counterstained with BoBo1. (E) Ctip2 immunostaining reveals layer V-VI neurons located 0-200 μm below the pia in the mutants. Sections counterstained with ToPro3. (F) Immunostaining for Tbr1 shows layer VI neurons positioned 100-200 μm below the mutant cortical surface. Arrowheads frame a population of Tbr1-positive axons coursing approximately 300 μm below the cortical surface in mutants. Sections counterstained with ToPro3. (G) Double-labeling with Tbr1 and Ctip2 in mutant sections demonstrates that Ctip2-positive layer V neurons (red) are positioned above double-positive (yellow) layer VI neurons. Arrows identify yellow double-stained nuclei. (H and I) Immunostaining for Tbr1 (H) and Smi32 (I) shows bundles of axons running transversely through the mutant neocortex. Dotted lines frame the axons. II/III, layers II-III; IV, layer IV; V, layer V; VI, layer VI; AX, axons; WM, white matter. Scale bars: 50 μm (A–C and G–I), 100 μm (D–F). See also Figure S7.

Dab1 Is Required Cell-Autonomously in Late-Born Neurons for Their Proper Positioning

Layering defects in the absence of reelin may be caused in part by defects in preplate splitting (Hoffarth et al., 1995; Sheppard and Pearlman, 1997); thus, reelin-dependent translocation may be required for preplate splitting, but not for layer formation per se. To test this hypothesis, we deleted *Dab1* after preplate splitting, only in late-born neurons. We generated *Cux2-CRE* mice driving recombination in neurons destined for layers II-IV (Nieto et al., 2004; Zimmer et al., 2004), but not V or VI (Figure S7). We then generated *Dab1*$^{flox/flox}$;*Cux2*$^{+/CRE}$ mice (referred to as *Dab1-CUX2ko*) (Figures 8A–8I). Immunohistochemistry for Map2

(Figures 8A and 8C) and CSPG (Figures 8B and 8C) showed that the preplate was split in *Dab1-Cux2ko* embryos, consistent with normal migration of early-born deep-layer neurons.

Next, we analyzed cell layers at P30. Staining for Cux1 (Figure 8D) revealed that late-born neurons were mislocalized deep in the *Dab1-CUX2ko* cortex. Because of this mislocalization, early-born neurons were displaced more superficially. However, their positions relative to each other were as in wild-type; layer V neurons positive for Ctip2 (Figures 8E and 8G) were located superficial to layer VI neurons positive for Tbr1 (Figures 8F and 8G). This was most obvious in sections double-stained for Citp2 and Tbr1 (Figure 8G). Additionally, a series of axons labeled by Tbr1 (Figure 8H) or Smi32 (Figure 8I) were found coursing beneath these early-born cells, suggesting that the subplate was positioned just below layer VI. Thus, only mutant neurons normally fated to layers II-IV failed to migrate past their wild-type predecessors and remained deep in the cortex of *Dab1-CUX2ko* mice. Therefore, even when the preplate is split, Dab1 is required cell-autonomously for proper lamination of later-born neurons.

DISCUSSION

We show here that Dab1-mediated reelin signaling regulates cortical lamination by controlling glia-independent somal translocation of early- and late-born neurons. In contrast, reelin signaling is not essential for glial-guided motility. A *reeler* phenotype is also observed when reelin signaling is disrupted in neurons alone without affecting RGCs, demonstrating that cell-autonomous neuronal deficits in somal translocation are sufficient to recapitulate the layering defect of the *reeler* phenotype. Finally, we show that glia-independent somal translocation depends on the Dab1 effector Rap1 and on Cdh2, and that migration defects caused by Rap1 inactivation are rescued by Cdh2 overexpression. These findings show that the Dab1 effector Rap1 regulates Cdh2 function to control glia-independent somal translocation, most likely by regulating the attachment of leading processes of migrating neurons.

While it is widely accepted that disturbances in glia-dependent migration cause cortical lamination defects, our findings demonstrate that loss of glia-independent motility is equally disruptive.

Models to explain the cortical lamination defect of *reeler* mice have mostly been based on the assumption that all radially migrating neurons move along RGC fibers. One prominent model proposes that reelin regulates detachment of neurons from RGC fibers to terminate migration. Consistent with this model, neurons in *reeler* mice accumulate along RGC fibers (Pinto-Lord et al., 1982) and invade the MZ (Caviness, 1982). Furthermore, perturbations in reelin signaling inhibit detachment of neurons from RGCs, possibly by regulating integrins (Dulabon et al., 2000; Sanada et al., 2004). However, integrins are not essential for cortical migration (Belvindrah et al., 2007) and early-born neurons largely migrate independently of RGCs (Nadarajah et al., 2001). In addition, migration is not arrested by diffusion of reelin through the cortical wall (Jossin et al., 2007) or by ectopic expression of reelin in the VZ (Magdaleno et al., 2002). Finally, several studies indicate that reelin in fact stimulates migration (Hashimoto-Torii et al., 2008; Jossin et al., 2004; Olson et al., 2006; Young-Pearse et al., 2007).

Taking into account the observations that cortical neurons migrate by glia-dependent and -independent modes, an alternative model has been proposed for reelin function: that reelin causes detachment of neurons from RGCs and stimulates terminal somal translocation (Cooper, 2008; Luque et al., 2003; Nadarajah et al., 2001). Using timed inactivation of reelin signaling, we now provide strong evidence for this model. We show that Dab1-mediated reelin signaling is essential for glia-independent somal translocation of both early- and late-born neurons, in which it stabilizes leading neuronal processes that are attached to the cortical MZ. Our findings can be reconciled with the observation that the adhesive properties of neurons are affected by perturbation of reelin signaling (Dulabon et al., 2000; Sanada et al., 2004) in that reelin induces branching of neuronal and RGC processes (Förster et al., 2002; Jossin and Goffinet, 2007; Niu et al., 2004; Pinto-Lord et al., 1982) and that the leading processes of translocating neurons exhibit branched morphologies once they contact the reelin-rich MZ (Nadarajah et al., 2001; Olson et al., 2006; Pinto-Lord et al., 1982).

We also provide insight into the signaling pathway by which reelin controls somal translocation. Dab1 is phosphorylated by SFKs upon reelin binding to its receptors (Arnaud et al., 2003; Howell et al., 1999). Phosphorylated Dab1 recruits several molecules, including PI3K (Bock et al., 2003) and Crk/CrkL/C3G (Ballif et al., 2004; Chen et al., 2004; Huang et al., 2004), which then regulate the activity of Limk1, Akt1, and Rap1 (Bock et al., 2003; Chai et al., 2009; Feng and Cooper, 2009; Jossin and Goffinet, 2007; Kuo et al., 2005; Park and Curran, 2008). It has been hypothesized that reelin stabilizes the actin cytoskeleton by inactivating N-cofilin through a Limk1-dependent pathway (Chai et al., 2009). However, when we perturb the function of Limk1 or N-cofilin, we do not affect migration. In agreement with these findings, early-born neurons migrate normally in N-cofilin mutant mice (Bellenchi et al., 2007) and Limk1 knockout mice have no cortical lamination defects (Meng et al., 2002). Likewise, we observed that inactivation of Akt does not affect migration. However, we show that Rap1, which is controlled by Crk/CrkL/C3G, is required for glia-independent translocation. These findings are in agreement with the results that Crk/CrkL double knockouts (Park and Curran, 2008) and C3G hypomorphs (Voss et al., 2008) phenocopy the lamination defects of *reeler* mice. We also provide evidence that Rap1 regulates cadherin function during migration and that inhibiting Rap1 or Cdh2 blocks somal translocation without affecting cell polarity. Migration defects caused by inactivation of Rap1 are rescued by overexpressing Cdh2, suggesting that Rap1 regulates cadherin function in migrating neurons. As Cdh2 levels in migrating neurons are regulated through endocytic pathways (Kawauchi et al., 2010), Rap1-mediated reelin signaling and endosomal trafficking may intersect. Finally, we anticipate that Rap1/cadherin is not the only pathway involved in reelin signaling, as glia-independent migration also requires cell body translocation and termination of migration. For example, Lis1 regulates nucleokinesis (Tsai et al., 2007) and binds Dab1 (Assadi et al., 2003), suggesting that reelin may control nuclear movement as well.

Our studies show that classical cadherins have broader roles in neocortical development than previously thought. Earlier studies have shown that Cdh2 and its β-catenin effector are

expressed in RGCs, where they regulate proliferation and neurogenesis (Brault et al., 2001; Kadowaki et al., 2007; Machon et al., 2003; Mutch et al., 2010; Woodhead et al., 2006; Zhang et al., 2010). Our findings show that Cdh2 in migrating neurons is required for glia-independent somal translocation, and recent findings suggest additional functions for classical cadherins in glial-guided motility (Kawauchi et al., 2010). The pleiotropic functions of Cdh2 in the neocortex indicate that its activity must be tightly controlled. Our findings suggest that reelin specifically controls Cdh2 function during glia-independent somal translocation, but other regulators still need to be identified. The Cdh2 cytoplasmic domain binds many proteins, raising the possibility that cadherin-dependent proliferation, differentiation, and migration in the CNS may depend on distinct effectors.

We also show that while components of the reelin pathway are expressed in RGCs and neurons (Luque et al., 2003; Magdaleno et al., 2002), positioning defects in Dab1 mutant mice are cell-autonomous to migrating neurons, as lamination defects of similar severity are observed in *Dab1-NESTINko* and *Dab1-NEXko* mice. Furthermore, we exclude that aberrantly positioned or overly adhesive subplate cells and deep-layer neurons (Hoffarth et al., 1995) are the primary cause for the migration defect in late-born neurons, as *Dab1-CUX2ko* mice exhibit normal preplate splitting but defective migration of late-born neurons. However, we do not exclude that nonautonomous defects also play a role. For example, in *Dab1-CUX2ko* mice, wild-type early-born neurons are positioned in the superficial half of the cortex instead of in their usual locations deep in the cortical wall, suggesting that final positioning and differentiation may depend on earlier-born neurons being passively displaced into deeper locations by later-born neurons.

It is interesting to note the relationship between terminal translocation and dendrite formation; two reelin regulated processes (Jossin and Goffinet, 2007; Niu et al., 2004; Olson et al., 2006). Translocation and dendritogenesis are initiated upon contact with the MZ and it is thought that the leading process of a migrating neuron is transformed into the apical dendrite (Pinto-Lord et al., 1982). Dendritogenesis has been proposed to be required for layer formation (Nichols and Olson, 2010). In this regard, our results from *Dab1-CUX2ko* mice provide interesting insight. Although the preplate is split in the mutants, layer I is thinner than in controls and layer V neurons occupy part of the space next to the pia. A similar phenotype is observed in *reeler* mice (Caviness, 1982; Sheppard and Pearlman, 1997), but in *Dab1-CUX2ko* mice the misplaced neurons are wild-type cells that are capable of transducing the reelin signal. Thus, it appears that the MZ is not invaded by unresponsive neurons in *Dab1-CUX2ko* mice. Instead, layer I is lost as a result of upper-layer mutant neurons failing to elaborate dendrites. It is therefore conceivable that reelin affects lamination by two processes: terminal translocation positions neurons and polarized dendritogenesis contributes to fine-tuning of layers.

EXPERIMENTAL PROCEDURES

Mice

For gene targeting see Supplemental Experimental Procedures. In brief, *Dab1^{flox}* mice were generated by flanking exon 2 of *Dab1* with LoxP sites. *Cux2-CRE* mice were generated by knocking CRE into the start ATG of *Cux2*. *Nestin-CRE* mice and *Nex-CRE* mice have been described (Graus-Porta et al., 2001) (Belvindrah et al., 2007; Goebbels et al., 2006).

Expression Constructs

For the generation of neuron-specific expression constructs, a characterized promoter fragment from the *Dcx* gene (Wang et al., 2007) was cloned into a vector containing an internal ribosome entry site (IRES) and EGFP. Coding sequences for various genes were inserted between the *Dcx* promoter and IRES-EGFP. shRNA expression vectors were from Open Biosystems. For details see Supplemental Experimental Procedures.

In Utero Electroporation

Timed pregnant mice were anesthetized and their uterine horns exposed. Plasmid DNA (2 μg ml^{-1}) was injected into the embryos' lateral ventricles. shRNA plasmids (1 μg ml^{-1}) were coinjected with a GFP expression vector (0.5 μg ml^{-1}). For electroporation, 5 pulses separated by 900 ms were applied at 38V for E12.5 embryos and at 50V for E15.5 embryos. Embryos were allowed to develop in utero for the indicated time. For analysis of embryos, brains were fixed in 4% paraformaldehyde (PFA) O/N at 4°C. For postnatal analysis, pups were fixed by transcardial perfusion with 4% PFA before dissection and fixation. Brains were sectioned coronally at 100 μm with a vibrating microtome (VT100S; Leica). At least four animals from three separate experiments were analyzed for each condition.

Histology

Nissl staining and immunohistology were performed as described (Belvindrah et al., 2007). An antibody list can be found in Supplemental Experimental Procedures. Sections were imaged with a laser-scanning confocal microscope. Image analysis was performed with MetaMorph (Molecular Devices). For quantification of layer markers, the neocortical wall was divided into ten equal-size bins; the number of positive nuclei in each bin was quantified and presented as % of the total number of cells in all ten bins, ± standard error of the mean (SEM). At least four animals from four experiments were analyzed for each condition. Electron microscopy details are in Supplemental Experimental Procedures.

Slice Culture and Time-Lapse Imaging

Dab1$^{flox/+}$ and *Dab1$^{flox/flox}$* embryos were electroporated with Dcx-CRE-iGFP at E15.5. 3 days later, embryos were dissected and brains processed for organotypic slice culture as described (Polleux and Ghosh, 2002). Time-lapse imaging was performed with an inverted spinning-disk confocal microscope (IX70; Olympus) with a temperature-controlled chamber containing 40% O_2 and 5% CO_2. An image z-stack ranging 9 μm was projected into a composite. Stacks were captured every 30 min for up to 96 hr. Image analysis was performed with MetaMorph. At least 12 slices from six brains in three separate experiments were analyzed for each condition. Quantification was carried out with at least 50 neurons for each genotype; statistical significance (p value) was calculated with Student's t test.

SUPPLEMENTAL INFORMATION

Supplemental Information includes seven figures, Supplemental Experimental Procedures, and eight movies and can be found with this article online at doi:10.1016/j.neuron.2011.01.003.

ACKNOWLEDGMENTS

We thank G. Bokoch, J. Cooper, M. Ginsberg, and S. Halpain for reagents; K. Spencer and M. Wood for microscopy help; C. Ramos, G. Martin, and S. Kupriyanov for assistance in generating mice; and N. Grillet for comments. This work was supported by the NIH (S.J.F., NS060355; U.M., NS046456, MH078833), Generalitat Valenciana (C.G.S., APOSTD/2010/064), Ministerio de Educacion (I.M.G., FU-2006-1238), the Skaggs Institute for Chemical Biology (U.M.), and the Dorris Neurscience Center (U.M.).

Accepted: January 4, 2011
Published: February 9, 2011

REFERENCES

Alcántara, S., Ruiz, M., D'Arcangelo, G., Ezan, F., de Lecea, L., Curran, T., Sotelo, C., and Soriano, E. (1998). Regional and cellular patterns of reelin mRNA expression in the forebrain of the developing and adult mouse. J. Neurosci. *18*, 7779–7799.

Arber, S., Barbayannis, F.A., Hanser, H., Schneider, C., Stanyon, C.A., Bernard, O., and Caroni, P. (1998). Regulation of actin dynamics through phosphorylation of cofilin by LIM-kinase. Nature *393*, 805–809.

Arnaud, L., Ballif, B.A., Förster, E., and Cooper, J.A. (2003). Fyn tyrosine kinase is a critical regulator of disabled-1 during brain development. Curr. Biol. *13*, 9–17.

Assadi, A.H., Zhang, G., Beffert, U., McNeil, R.S., Renfro, A.L., Niu, S., Quattrocchi, C.C., Antalffy, B.A., Sheldon, M., Armstrong, D.D., et al. (2003). Interaction of reelin signaling and Lis1 in brain development. Nat. Genet. *35*, 270–276.

Bai, J., Ramos, R.L., Ackman, J.B., Thomas, A.M., Lee, R.V., and LoTurco, J.J. (2003). RNAi reveals doublecortin is required for radial migration in rat neocortex. Nat. Neurosci. *6*, 1277–1283.

Ballif, B.A., Arnaud, L., Arthur, W.T., Guris, D., Imamoto, A., and Cooper, J.A. (2004). Activation of a Dab1/CrkL/C3G/Rap1 pathway in Reelin-stimulated neurons. Curr. Biol. *14*, 606–610.

Bellenchi, G.C., Gurniak, C.B., Perlas, E., Middei, S., Ammassari-Teule, M., and Witke, W. (2007). N-cofilin is associated with neuronal migration disorders and cell cycle control in the cerebral cortex. Genes Dev. *21*, 2347–2357.

Belvindrah, R., Graus-Porta, D., Goebbels, S., Nave, K.A., and Müller, U. (2007). Beta1 integrins in radial glia but not in migrating neurons are essential for the formation of cell layers in the cerebral cortex. J. Neurosci. *27*, 13854–13865.

Bock, H.H., Jossin, Y., Liu, P., Förster, E., May, P., Goffinet, A.M., and Herz, J. (2003). Phosphatidylinositol 3-kinase interacts with the adaptor protein Dab1 in response to Reelin signaling and is required for normal cortical lamination. J. Biol. Chem. *278*, 38772–38779.

Brault, V., Moore, R., Kutsch, S., Ishibashi, M., Rowitch, D.H., McMahon, A.P., Sommer, L., Boussadia, O., and Kemler, R. (2001). Inactivation of the beta-catenin gene by Wnt1-Cre-mediated deletion results in dramatic brain malformation and failure of craniofacial development. Development *128*, 1253–1264.

Caviness, V.S., Jr. (1982). Neocortical histogenesis in normal and reeler mice: A developmental study based upon [3H]thymidine autoradiography. Brain Res. *256*, 293–302.

Chae, T., Kwon, Y.T., Bronson, R., Dikkes, P., Li, E., and Tsai, L.H. (1997). Mice lacking p35, a neuronal specific activator of Cdk5, display cortical lamination defects, seizures, and adult lethality. Neuron *18*, 29–42.

Chai, X., Förster, E., Zhao, S., Bock, H.H., and Frotscher, M. (2009). Reelin stabilizes the actin cytoskeleton of neuronal processes by inducing n-cofilin phosphorylation at serine3. J. Neurosci. *29*, 288–299.

Chen, K., Ochalski, P.G., Tran, T.S., Sahir, N., Schubert, M., Pramatarova, A., and Howell, B.W. (2004). Interaction between Dab1 and CrkII is promoted by Reelin signaling. J. Cell Sci. *117*, 4527–4536.

Chenn, A., and Walsh, C.A. (2002). Regulation of cerebral cortical size by control of cell cycle exit in neural precursors. Science *297*, 365–369.

Cooper, J.A. (2008). A mechanism for inside-out lamination in the neocortex. Trends Neurosci. *31*, 113–119.

D'Arcangelo, G., Nakajima, K., Miyata, T., Ogawa, M., Mikoshiba, K., and Curran, T. (1997). Reelin is a secreted glycoprotein recognized by the CR-50 monoclonal antibody. J. Neurosci. *17*, 23–31.

D'Arcangelo, G., Homayouni, R., Keshvara, L., Rice, D.S., Sheldon, M., and Curran, T. (1999). Reelin is a ligand for lipoprotein receptors. Neuron *24*, 471–479.

Dulabon, L., Olson, E.C., Taglienti, M.G., Eisenhuth, S., McGrath, B., Walsh, C.A., Kreidberg, J.A., and Anton, E.S. (2000). Reelin binds alpha3beta1 integrin and inhibits neuronal migration. Neuron *27*, 33–44.

Edwards, D.C., and Gill, G.N. (1999). Structural features of LIM kinase that control effects on the actin cytoskeleton. J. Biol. Chem. *274*, 11352–11361.

Feng, L., and Cooper, J.A. (2009). Dual functions of Dab1 during brain development. Mol. Cell. Biol. *29*, 324–332.

Förster, E., Tielsch, A., Saum, B., Weiss, K.H., Johanssen, C., Graus-Porta, D., Müller, U., and Frotscher, M. (2002). Reelin, Disabled 1, and beta 1 integrins are required for the formation of the radial glial scaffold in the hippocampus. Proc. Natl. Acad. Sci. USA *99*, 13178–13183.

Franke, T.F., Yang, S.I., Chan, T.O., Datta, K., Kazlauskas, A., Morrison, D.K., Kaplan, D.R., and Tsichlis, P.N. (1995). The protein kinase encoded by the Akt proto-oncogene is a target of the PDGF-activated phosphatidylinositol 3-kinase. Cell *81*, 727–736.

Gilmore, E.C., and Herrup, K. (2000). Cortical development: Receiving reelin. Curr. Biol. *10*, R162–R166.

Gilmore, E.C., Ohshima, T., Goffinet, A.M., Kulkarni, A.B., and Herrup, K. (1998). Cyclin-dependent kinase 5-deficient mice demonstrate novel developmental arrest in cerebral cortex. J. Neurosci. *18*, 6370–6377.

Goebbels, S., Bormuth, I., Bode, U., Hermanson, O., Schwab, M.H., and Nave, K.A. (2006). Genetic targeting of principal neurons in neocortex and hippocampus of NEX-Cre mice. Genesis *44*, 611–621.

Graus-Porta, D., Blaess, S., Senften, M., Littlewood-Evans, A., Damsky, C., Huang, Z., Orban, P., Klein, R., Schittny, J.C., and Müller, U. (2001). Beta1-class integrins regulate the development of laminae and folia in the cerebral and cerebellar cortex. Neuron *31*, 367–379.

Han, J., Lim, C.J., Watanabe, N., Soriani, A., Ratnikov, B., Calderwood, D.A., Puzon-McLaughlin, W., Lafuente, E.M., Boussiotis, V.A., Shattil, S.J., and Ginsberg, M.H. (2006). Reconstructing and deconstructing agonist-induced activation of integrin alphaIIbbeta3. Curr. Biol. *16*, 1796–1806.

Hartfuss, E., Förster, E., Bock, H.H., Hack, M.A., Leprince, P., Luque, J.M., Herz, J., Frotscher, M., and Götz, M. (2003). Reelin signaling directly affects radial glia morphology and biochemical maturation. Development *130*, 4597–4609.

Hashimoto-Torii, K., Torii, M., Sarkisian, M.R., Bartley, C.M., Shen, J., Radtke, F., Gridley, T., Sestan, N., and Rakic, P. (2008). Interaction between Reelin and Notch signaling regulates neuronal migration in the cerebral cortex. Neuron *60*, 273–284.

Herrick, T.M., and Cooper, J.A. (2002). A hypomorphic allele of dab1 reveals regional differences in reelin-Dab1 signaling during brain development. Development *129*, 787–796.

Hiesberger, T., Trommsdorff, M., Howell, B.W., Goffinet, A., Mumby, M.C., Cooper, J.A., and Herz, J. (1999). Direct binding of Reelin to VLDL receptor and ApoE receptor 2 induces tyrosine phosphorylation of disabled-1 and modulates tau phosphorylation. Neuron *24*, 481–489.

Hoffarth, R.M., Johnston, J.G., Krushel, L.A., and van der Kooy, D. (1995). The mouse mutation reeler causes increased adhesion within a subpopulation of early postmitotic cortical neurons. J. Neurosci. *15*, 4838–4850.

Hong, S.E., Shugart, Y.Y., Huang, D.T., Shahwan, S.A., Grant, P.E., Hourihane, J.O., Martin, N.D., and Walsh, C.A. (2000). Autosomal recessive lissencephaly with cerebellar hypoplasia is associated with human RELN mutations. Nat. Genet. *26*, 93–96.

Howell, B.W., Hawkes, R., Soriano, P., and Cooper, J.A. (1997). Neuronal position in the developing brain is regulated by mouse disabled-1. Nature *389*, 733–737.

Howell, B.W., Herrick, T.M., and Cooper, J.A. (1999). Reelin-induced tyrosine [corrected] phosphorylation of disabled 1 during neuronal positioning. Genes Dev. *13*, 643–648.

Howell, B.W., Herrick, T.M., Hildebrand, J.D., Zhang, Y., and Cooper, J.A. (2000). Dab1 tyrosine phosphorylation sites relay positional signals during mouse brain development. Curr. Biol. *10*, 877–885.

Huang, Y., Magdaleno, S., Hopkins, R., Slaughter, C., Curran, T., and Keshvara, L. (2004). Tyrosine phosphorylated Disabled 1 recruits Crk family adapter proteins. Biochem. Biophys. Res. Commun. *318*, 204–212.

Hunter-Schaedle, K.E. (1997). Radial glial cell development and transformation are disturbed in reeler forebrain. J. Neurobiol. *33*, 459–472.

Jossin, Y., and Goffinet, A.M. (2007). Reelin signals through phosphatidylinositol 3-kinase and Akt to control cortical development and through mTor to regulate dendritic growth. Mol. Cell. Biol. *27*, 7113–7124.

Jossin, Y., Ignatova, N., Hiesberger, T., Herz, J., Lambert de Rouvroit, C., and Goffinet, A.M. (2004). The central fragment of Reelin, generated by proteolytic processing in vivo, is critical to its function during cortical plate development. J. Neurosci. *24*, 514–521.

Jossin, Y., Gui, L., and Goffinet, A.M. (2007). Processing of Reelin by embryonic neurons is important for function in tissue but not in dissociated cultured neurons. J. Neurosci. *27*, 4243–4252.

Kadowaki, M., Nakamura, S., Machon, O., Krauss, S., Radice, G.L., and Takeichi, M. (2007). N-cadherin mediates cortical organization in the mouse brain. Dev. Biol. *304*, 22–33.

Kawauchi, T., Sekine, K., Shikanai, M., Chihama, K., Tomita, K., Kubo, K., Nakajima, K., Nabeshima, Y., and Hoshino, M. (2010). Rab GTPases-dependent endocytic pathways regulate neuronal migration and maturation through N-cadherin trafficking. Neuron *67*, 588–602.

Ko, J., Humbert, S., Bronson, R.T., Takahashi, S., Kulkarni, A.B., Li, E., and Tsai, L.H. (2001). p35 and p39 are essential for cyclin-dependent kinase 5 function during neurodevelopment. J. Neurosci. *21*, 6758–6771.

Kooistra, M.R., Dubé, N., and Bos, J.L. (2007). Rap1: A key regulator in cell-cell junction formation. J. Cell Sci. *120*, 17–22.

Kuo, G., Arnaud, L., Kronstad-O'Brien, P., and Cooper, J.A. (2005). Absence of Fyn and Src causes a reeler-like phenotype. J. Neurosci. *25*, 8578–8586.

Landrieu, P., and Goffinet, A. (1981). Inverted pyramidal neurons and their axons in the neocortex of reeler mutant mice. Cell Tissue Res. *218*, 293–301.

Luque, J.M., Morante-Oria, J., and Fairén, A. (2003). Localization of ApoER2, VLDLR and Dab1 in radial glia: Groundwork for a new model of reelin action during cortical development. Brain Res. Dev. Brain Res. *140*, 195–203.

Machon, O., van den Bout, C.J., Backman, M., Kemler, R., and Krauss, S. (2003). Role of beta-catenin in the developing cortical and hippocampal neuroepithelium. Neuroscience *122*, 129–143.

Magdaleno, S., Keshvara, L., and Curran, T. (2002). Rescue of ataxia and preplate splitting by ectopic expression of Reelin in reeler mice. Neuron *33*, 573–586.

Meng, Y., Zhang, Y., Tregoubov, V., Janus, C., Cruz, L., Jackson, M., Lu, W.Y., MacDonald, J.F., Wang, J.Y., Falls, D.L., and Jia, Z. (2002). Abnormal spine morphology and enhanced LTP in LIMK-1 knockout mice. Neuron *35*, 121–133.

Miyata, T., Kawaguchi, A., Okano, H., and Ogawa, M. (2001). Asymmetric inheritance of radial glial fibers by cortical neurons. Neuron *31*, 727–741.

Morest, D.K. (1970). A study of neurogenesis in the forebrain of opossum pouch young. Z. Anat. Entwicklungsgesch. *130*, 265–305.

Mutch, C.A., Schulte, J.D., Olson, E., and Chenn, A. (2010). Beta-catenin signaling negatively regulates intermediate progenitor population numbers in the developing cortex. PLoS ONE *5*, e12376.

Nadarajah, B., Brunstrom, J.E., Grutzendler, J., Wong, R.O., and Pearlman, A.L. (2001). Two modes of radial migration in early development of the cerebral cortex. Nat. Neurosci. *4*, 143–150.

Nagaoka, R., Abe, H., and Obinata, T. (1996). Site-directed mutagenesis of the phosphorylation site of cofilin: Its role in cofilin-actin interaction and cytoplasmic localization. Cell Motil. Cytoskeleton *35*, 200–209.

Nichols, A.J., and Olson, E.C. (2010). Reelin Promotes neuronal orientation and dendritogenesis during preplate splitting. Cereb. Cortex *20*, 2213–2223.

Nieto, M., Monuki, E.S., Tang, H., Imitola, J., Haubst, N., Khoury, S.J., Cunningham, J., Gotz, M., and Walsh, C.A. (2004). Expression of Cux-1 and Cux-2 in the subventricular zone and upper layers II-IV of the cerebral cortex. J. Comp. Neurol. *479*, 168–180.

Niu, S., Renfro, A., Quattrocchi, C.C., Sheldon, M., and D'Arcangelo, G. (2004). Reelin promotes hippocampal dendrite development through the VLDLR/ApoER2-Dab1 pathway. Neuron *41*, 71–84.

Noctor, S.C., Martínez-Cerdeño, V., Ivic, L., and Kriegstein, A.R. (2004). Cortical neurons arise in symmetric and asymmetric division zones and migrate through specific phases. Nat. Neurosci. *7*, 136–144.

Ogawa, M., Miyata, T., Nakajima, K., Yagyu, K., Seike, M., Ikenaka, K., Yamamoto, H., and Mikoshiba, K. (1995). The reeler gene-associated antigen on Cajal-Retzius neurons is a crucial molecule for laminar organization of cortical neurons. Neuron *14*, 899–912.

Olson, E.C., Kim, S., and Walsh, C.A. (2006). Impaired neuronal positioning and dendritogenesis in the neocortex after cell-autonomous Dab1 suppression. J. Neurosci. *26*, 1767–1775.

Park, T.J., and Curran, T. (2008). Crk and Crk-like play essential overlapping roles downstream of disabled-1 in the Reelin pathway. J. Neurosci. *28*, 13551–13562.

Pinto-Lord, M.C., Evrard, P., and Caviness, V.S., Jr. (1982). Obstructed neuronal migration along radial glial fibers in the neocortex of the reeler mouse: A Golgi-EM analysis. Brain Res. *256*, 379–393.

Polleux, F., and Ghosh, A. (2002). The slice overlay assay: A versatile tool to study the influence of extracellular signals on neuronal development. Sci. STKE *2002*, pl9.

Rakic, P. (1972). Mode of cell migration to the superficial layers of fetal monkey neocortex. J. Comp. Neurol. *145*, 61–83.

Rice, D.S., and Curran, T. (2001). Role of the reelin signaling pathway in central nervous system development. Annu. Rev. Neurosci. *24*, 1005–1039.

Rice, D.S., Sheldon, M., D'Arcangelo, G., Nakajima, K., Goldowitz, D., and Curran, T. (1998). Disabled-1 acts downstream of Reelin in a signaling pathway that controls laminar organization in the mammalian brain. Development *125*, 3719–3729.

Rubinfeld, B., Crosier, W.J., Albert, I., Conroy, L., Clark, R., McCormick, F., and Polakis, P. (1992). Localization of the rap1GAP catalytic domain and sites of phosphorylation by mutational analysis. Mol. Cell. Biol. *12*, 4634–4642.

Sanada, K., Gupta, A., and Tsai, L.H. (2004). Disabled-1-regulated adhesion of migrating neurons to radial glial fiber contributes to neuronal positioning during early corticogenesis. Neuron *42*, 197–211.

Schiffmann, S.N., Bernier, B., and Goffinet, A.M. (1997). Reelin mRNA expression during mouse brain development. Eur. J. Neurosci. *9*, 1055–1071.

Sheldon, M., Rice, D.S., D'Arcangelo, G., Yoneshima, H., Nakajima, K., Mikoshiba, K., Howell, B.W., Cooper, J.A., Goldowitz, D., and Curran, T. (1997). Scrambler and yotari disrupt the disabled gene and produce a reeler-like phenotype in mice. Nature *389*, 730–733.

Sheppard, A.M., and Pearlman, A.L. (1997). Abnormal reorganization of preplate neurons and their associated extracellular matrix: An early manifestation of altered neocortical development in the reeler mutant mouse. J. Comp. Neurol. *378*, 173–179.

Shoukimas, G.M., and Hinds, J.W. (1978). The development of the cerebral cortex in the embryonic mouse: An electron microscopic serial section analysis. J. Comp. Neurol. *179*, 795–830.

Shu, T., Ayala, R., Nguyen, M.D., Xie, Z., Gleeson, J.G., and Tsai, L.H. (2004). Ndel1 operates in a common pathway with LIS1 and cytoplasmic dynein to regulate cortical neuronal positioning. Neuron *44*, 263–277.

Tabata, H., and Nakajima, K. (2003). Multipolar migration: The third mode of radial neuronal migration in the developing cerebral cortex. J. Neurosci. *23*, 9996–10001.

Tabata, H., Kanatani, S., and Nakajima, K. (2009). Differences of migratory behavior between direct progeny of apical progenitors and basal progenitors in the developing cerebral cortex. Cereb. Cortex *19*, 2092–2105.

Trommsdorff, M., Gotthardt, M., Hiesberger, T., Shelton, J., Stockinger, W., Nimpf, J., Hammer, R.E., Richardson, J.A., and Herz, J. (1999). Reeler/

Disabled-like disruption of neuronal migration in knockout mice lacking the VLDL receptor and ApoE receptor 2. Cell *97*, 689–701.

Tsai, J.W., Bremner, K.H., and Vallee, R.B. (2007). Dual subcellular roles for LIS1 and dynein in radial neuronal migration in live brain tissue. Nat. Neurosci. *10*, 970–979.

Voss, A.K., Britto, J.M., Dixon, M.P., Sheikh, B.N., Collin, C., Tan, S.S., and Thomas, T. (2008). C3G regulates cortical neuron migration, preplate splitting and radial glial cell attachment. Development *135*, 2139–2149.

Wang, X., Qiu, R., Tsark, W., and Lu, Q. (2007). Rapid promoter analysis in developing mouse brain and genetic labeling of young neurons by doublecortin-DsRed-express. J. Neurosci. Res. *85*, 3567–3573.

Ware, M.L., Fox, J.W., González, J.L., Davis, N.M., Lambert de Rouvroit, C., Russo, C.J., Chua, S.C., Jr., Goffinet, A.M., and Walsh, C.A. (1997). Aberrant splicing of a mouse disabled homolog, mdab1, in the scrambler mouse. Neuron *19*, 239–249.

Woodhead, G.J., Mutch, C.A., Olson, E.C., and Chenn, A. (2006). Cell-autonomous beta-catenin signaling regulates cortical precursor proliferation. J. Neurosci. *26*, 12620–12630.

Yang, N., Higuchi, O., Ohashi, K., Nagata, K., Wada, A., Kangawa, K., Nishida, E., and Mizuno, K. (1998). Cofilin phosphorylation by LIM-kinase 1 and its role in Rac-mediated actin reorganization. Nature *393*, 809–812.

Young-Pearse, T.L., Bai, J., Chang, R., Zheng, J.B., LoTurco, J.J., and Selkoe, D.J. (2007). A critical function for beta-amyloid precursor protein in neuronal migration revealed by in utero RNA interference. J. Neurosci. *27*, 14459–14469.

Zhang, J., Woodhead, G.J., Swaminathan, S.K., Noles, S.R., McQuinn, E.R., Pisarek, A.J., Stocker, A.M., Mutch, C.A., Funatsu, N., and Chenn, A. (2010). Cortical neural precursors inhibit their own differentiation via N-cadherin maintenance of beta-catenin signaling. Dev. Cell *18*, 472–479.

Zimmer, C., Tiveron, M.C., Bodmer, R., and Cremer, H. (2004). Dynamics of Cux2 expression suggests that an early pool of SVZ precursors is fated to become upper cortical layer neurons. Cereb. Cortex *14*, 1408–1420.

Neuron, Volume *69*

Supplemental Information

Reelin Regulates Cadherin Function via Dab1/Rap1 to Control Neuronal Migration and Lamination in the Neocortex

Santos J. Franco, Isabel Martinez-Garay, Cristina Gil-Sanz, Sarah R. Harkins-Perry, and Ulrich Müller

Figure S1, related to Figure 1 (Franco, et. al.)

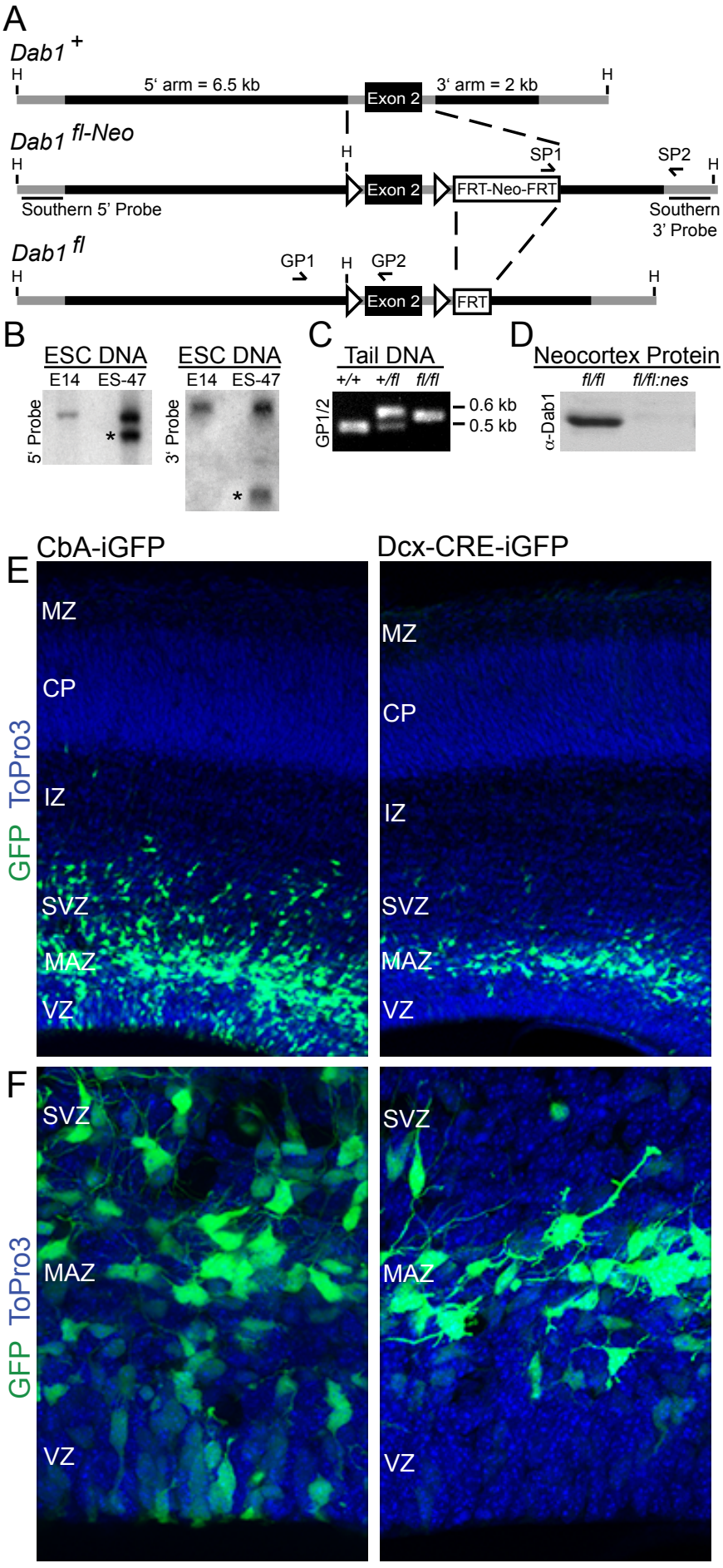

Figure S1. (A-D) Generation and characterization of a conditional Dab1 allele. **(A)** Schematic diagram of wild-type (+) and floxed (*fl-Neo, fl*) alleles of the *Dab1* gene. Thick black bars represent DNA segments used for constructing the targeting vector; gray bars identify flanking genomic DNA. Relevant restriction sites (H, HindIII), Southern probes (thin black bars) and PCR primers for screening (SP1, SP2) and genotyping (GP1, GP2) are indicated. **(B)** Southern blot analysis of targeted ES cells. Genomic DNA from wild-type (E14) and targeted (ES-47) ES cells was digested with HindIII and hybridized with 5’ and 3’ external probes. Star (*) indicates the targeted *fl-Neo* allele. **(C)** PCR analysis of floxed *Dab1* mice. Genomic DNA from wild-type, heterozygous and homozygous *Dab1-fl* mouse tails was analyzed using genotyping primers GP1 and GP2. **(D)** Loss of Dab1 protein upon CNS-wide expression of CRE recombinase from the *Nestin-CRE* transgene. Representative immunoblot of neocortical tissue from E16.5 homozygous *Dab1-fl* mice without (*fl/fl*) or with (*fl/fl;nes*) the *Nestin-CRE* transgene. **(E-F)** Neuron-specific expression from the *Dcx* promoter after *in utero* electroporation. **(E)** Wild-type embryos were electroporated at E14.5 and analyzed at E16.5. Left panel, cortical sections from embryos electroporated with a plasmid in which EGFP is expressed constitutively from the chicken β-actin promoter (CbA). Right panel, coronal sections from embryos electroporated with Dcx-CRE-iGFP in which Cre and EGFP are expressed from a mouse doublecortin promoter fragment. Sections are counterstained with ToPro3 to reveal cortical cytoarchitecture. Note the absence of GFP expression in the VZ with Dcx-CRE-iGFP compared to CbA-iGFP. **(F)** Higher magnification of the VZ from images shown in **(E)**. CP, cortical plate; IZ, intermediate zone; MAZ; multipolar accumulation zone; MZ, marginal zone; SVZ, subventricular zone; VZ, ventricular zone.

Figure S2, related to Figure 2 (Franco, et. al.)

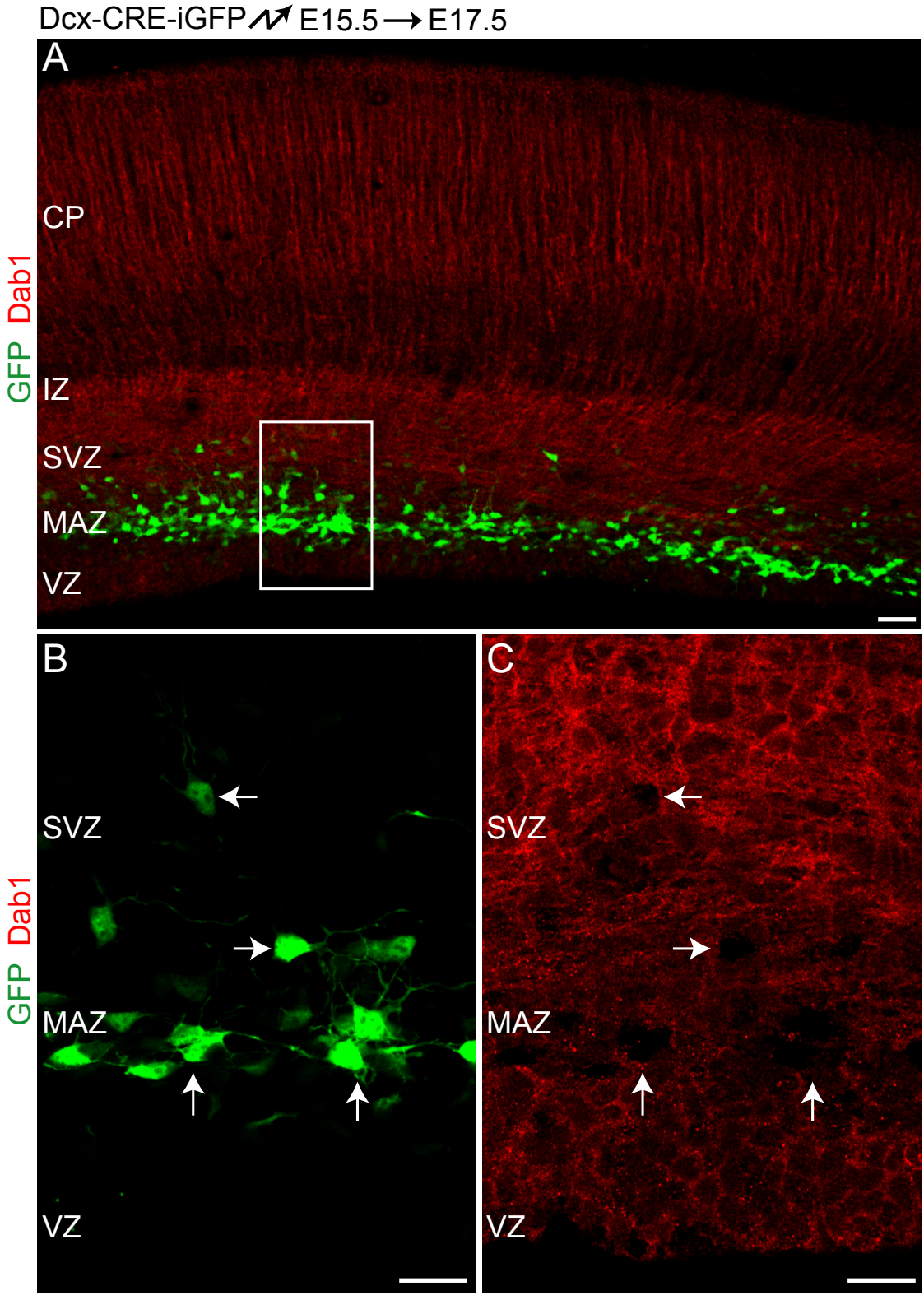

Figure S2. Loss of Dab1 protein after in utero electroporation of Dcx-CRE-iGFP into *Dab1-fl/fl* embryos. **(A)** Immunostaining for Dab1 two days (E17.5) after electroporation of Dcx-CRE-iGFP into *Dab1-fl/fl* embryos at E15.5. **(B-C)** High magnification single channel images of the boxed area shown in **(A)**. Arrows point to GFP-positive **(B)** electroporated cells that have decreased Dab1 immunoreactivity **(C)** compared to surrounding, untransfected cells. Scale bars represent 100 μm **(A)** and 50 μm **(B-C)**.

Figure S3, related to Figure 3 (Franco, et. al.)

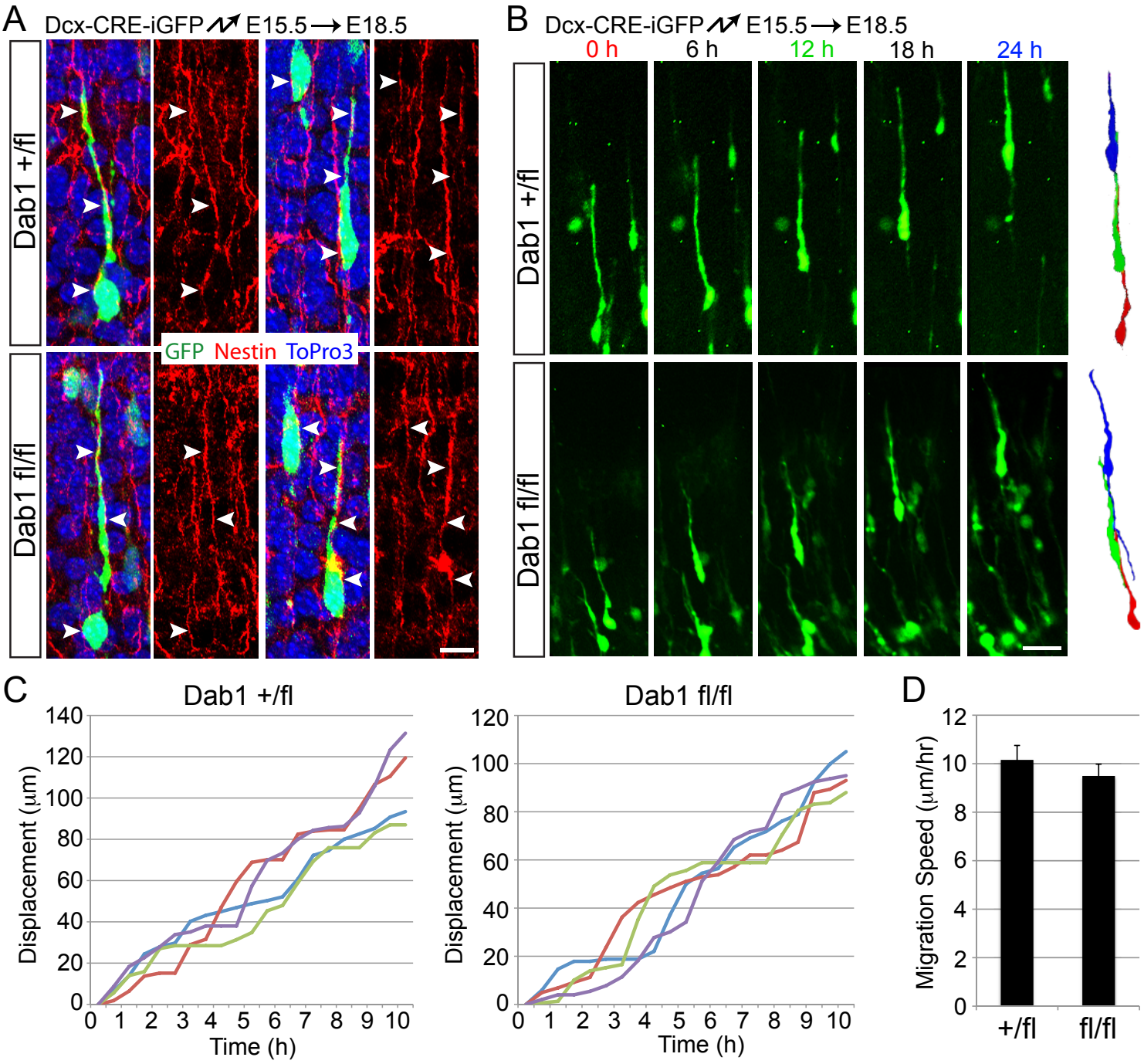

Figure S3. Dab1 is not required for glia-guided locomotion. **(A)** Normal neuron-glia interactions of Dab1-deficient neurons. Coronal sections from heterozygous (top panels) and homozygous (bottom panels) Dab1-flox embryos electroporated with Dcx-CRE-iGFP at E15.5 and analyzed at E18.5. Immunostaining for nestin shows electroporated neurons (green) in close apposition to nestin-positive RGC fibers (red) in the IZ (left panels) and CP (right panels) in control and mutant brains. **(B-D)** Glia-guided locomotion is unaffected by loss of Dab1. *Dab1+/fl* and *Dab1fl/fl* embryos were electroporated with Dcx-CRE-iGFP at E15.5, processed for slice cultures at E18.5, and imaged by spinning-disk confocal time-lapse microscopy. **(B)** Representative images from time-lapse experiments tracking the motility of electroporated neurons during glia-guided locomotion through the lower CP. To the right of each series, traces represent the migrating neurons at 0 h (red), 12 h (green) and 24 h (blue). **(C)** Traces of 4 control (left) and mutant (right) neurons migrating by glia-guided locomotion over a 10 hour period. Control and mutant neurons display saltatory movement in the lower CP. **(D)** Quantification of average migration speed of neurons undergoing glia-guided locomotion; Control = 10.1 ± 3.2 [s.d.] µm/hr, Mutant = 9.5 ± 3.6 [s.d.] µm/hr; P = 0.39 by t-test. Scale bars: 10 µm **(A)** and 25 µm **(B)**.

Figure S4, related to Figure 5 (Franco, et. al.)

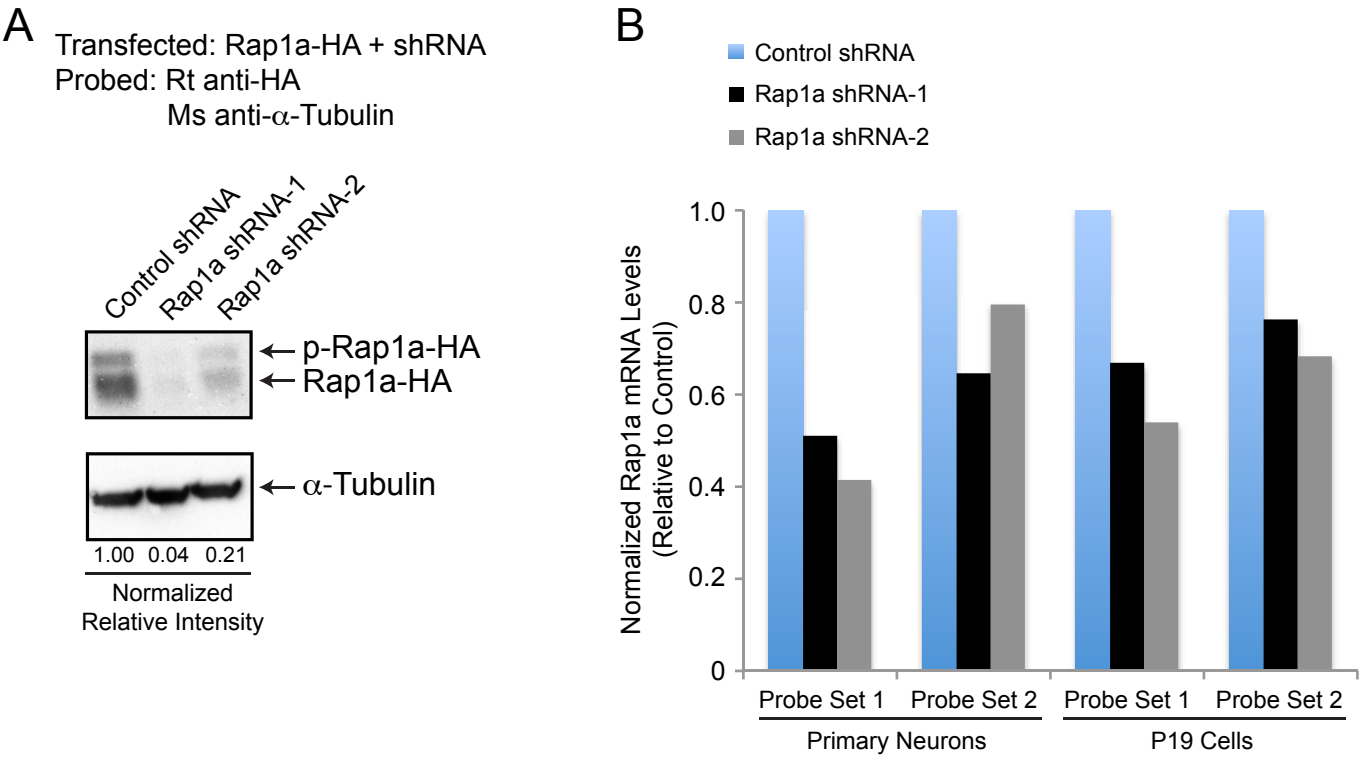

Figure S4. shRNA-mediated knockdown of Rap1a protein and mRNA. **(A)** Reduction of exogenously expressed Rap1a protein. Western blot showing reduction of HA-tagged Rap1a (Rap1a-HA) protein in lysates from 293T cells transfected with Rap1a-HA and shRNA constructs targeting mouse Rap1a, compared to lysates from cells transfected with Rap1a-HA and a non-silencing control shRNA. Blot was probed with anti-HA antibody followed by anti-α-tubulin as a loading control. Rap1a-HA signal was normalized to tubulin and quantified relative to control. **(B)** Reduction of endogenous Rap1a mRNA. Graph of quantitative RT-PCR results showing shRNA-mediated knockdown of endogenous Rap1a mRNA in primary neurons and P19 cells. Rap1a-specific or non-silencing control shRNAs were nucleofected into primary cortical neurons from E14.5 mouse embryos, or transfected into P19 cells, and RNA was harvested 48 hours later. Graph shows two different Rap1a-specific probe sets for each cell type. mRNA levels were normalized to a GAPDH control probe set and graphed relative to control shRNA samples.

Figure S5, related to Figure 6 (Franco, et. al.)

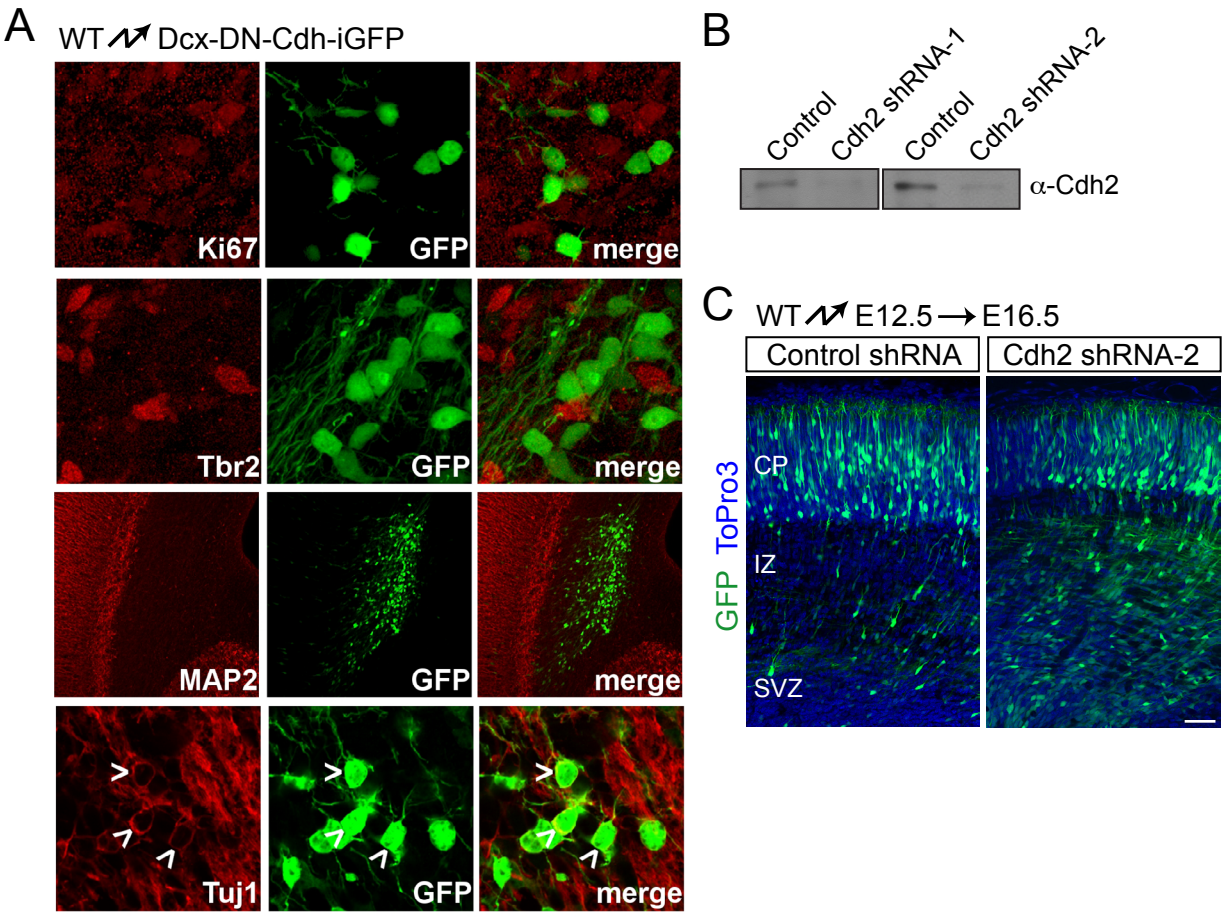

Figure S5. Controls for dominant-negative cadherin and Cdh2 shRNA. **(A)** DN-cadherin expressed from the Dcx promoter is expressed only in immature neurons. Dcx-DN-cadherin-iGFP was electroporated *in utero* and embryos were analyzed 2 days later. Immunohistochemical analysis revealed GFP+ cells were negative for Ki67, Tbr2 and Map2, demonstrating that electroporated cells were not proliferating, not intermediate progenitors and not mature neurons, respectively. Positive staining for Tuj1 (open arrowheads) shows that electroporated cells are immature neurons. **(B)** Reduction of Cdh2 protein by shRNA-mediated knockdown. Western blots probed with a Cdh2 antibody showing decreased Cdh2 protein levels after nucleofection of primary cortical neurons with either of two Cdh2-specific shRNA constructs. **(C)** Coronal sections from embryos electroporated at E12.5 with non-silencing control or an shRNA construct targeting Cdh2. Analysis performed at E16.5. Scale bar, 50 μm.

Figure S6, related to Figure 7 (Franco, et. al.)

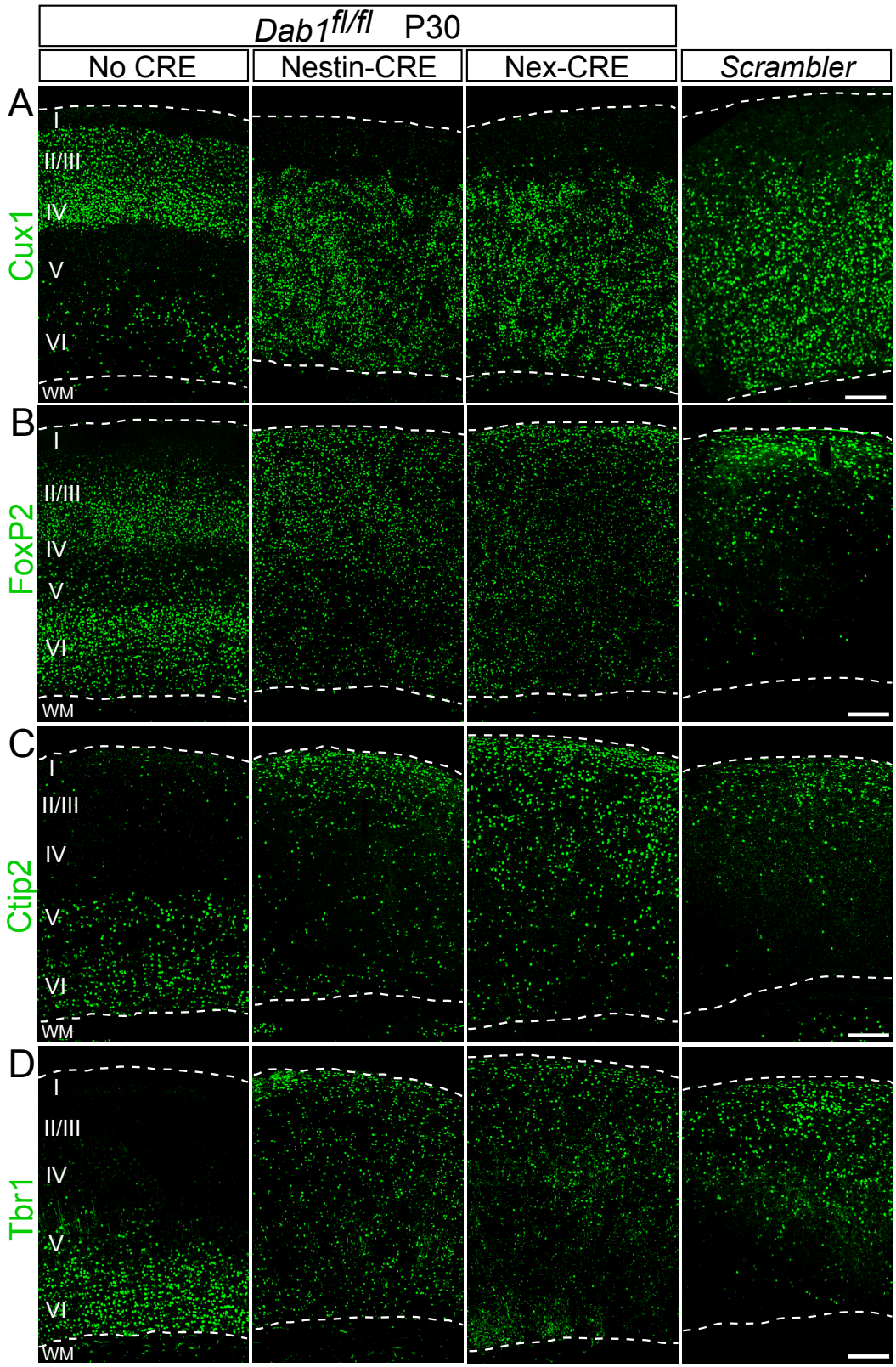

Figure S6. Similar neocortical lamination defects in *Dab1-NESTINko* and *Dab1-NEXko* mutant mice. (**A-D**) Immunostaining for neocortical layer markers at P30 in *Dab1fl/fl* (No CRE), *Dab1-NESTINko* (Nestin-CRE), *Dab1-NEXko* (Nex-CRE), and *Scrambler* mice. (**A**) Cux1 immunostaining reveals neurons that normally occupy layers II-IV. (**B**) FoxP2 stains primarily layer VI neurons and a subset of layer III/IV neurons. (**C**) Ctip2 labels neurons in layers V and VI. (**D**) Tbr1 stains layer VI neurons. Top dotted lines represent the pial surface and lower dotted lines outline the borders between layer VI and the white matter; ToPro3 counterstain (not shown) was used to identify these landmarks. Cortical layers are labeled I-VI. WM, white matter. Scale bars: 200 μm.

Figure S7, related to Figure 8 (Franco, et. al.)

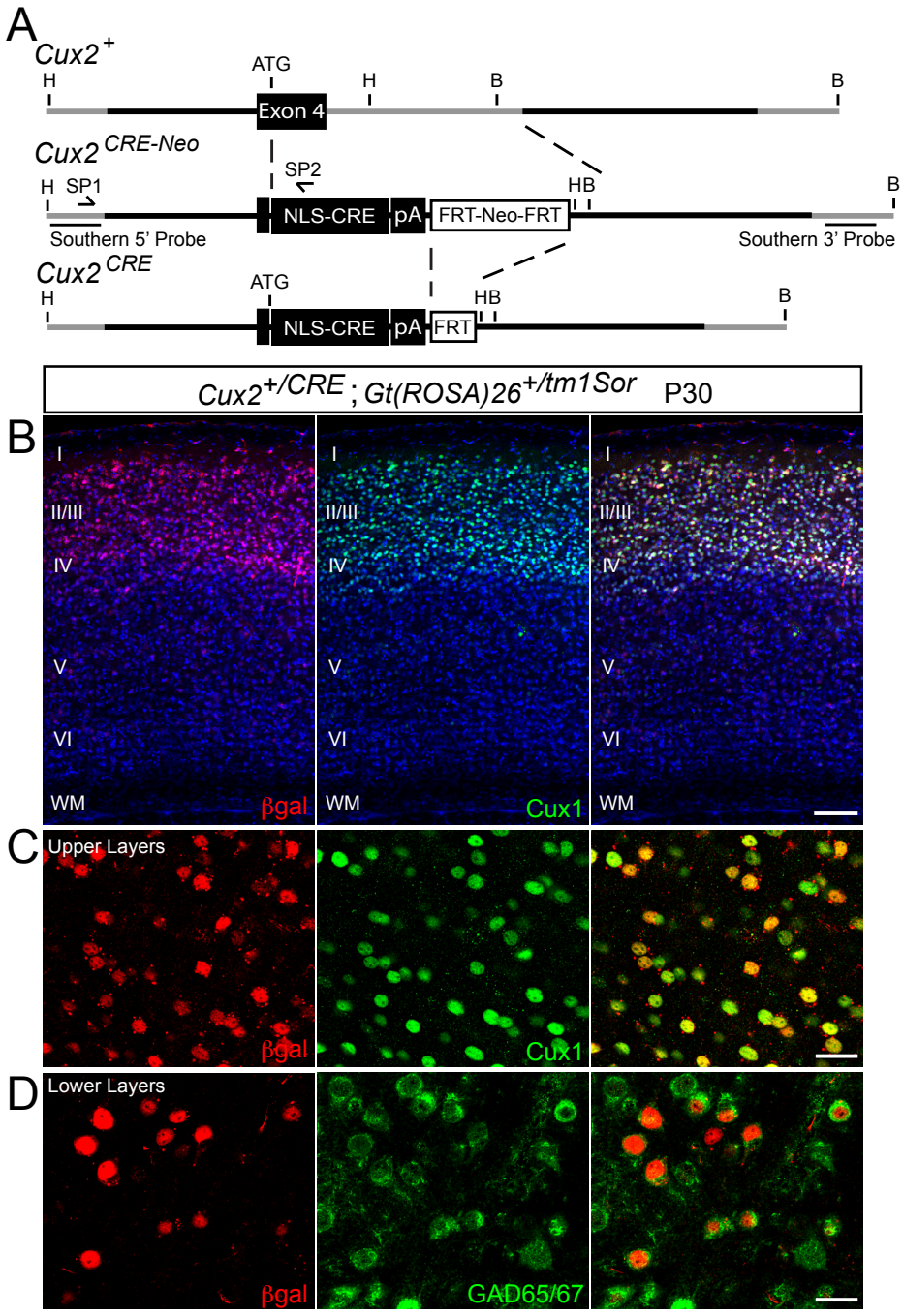

Figure S7. Generation and characterization of *Cux2-CRE* mice. **(A)** Schematic diagram of wild-type (+) and CRE (*CRE-Neo, CRE*) alleles of the *Cux2* gene. Thick black bars represent DNA segments used for constructing the targeting vector; gray bars identify flanking genomic DNA. Relevant restriction sites (B, BamHI; H, HindIII), Southern probes (thin black bars) and PCR primers for screening (SP1, SP2) and genotyping (GP1, GP2) are indicated. **(B)** CRE-mediated recombination in upper-layer neurons in *Cux2-CRE* mice. *Cux2-CRE* mice were mated to the *Rosa26R* LacZ reporter strain and analyzed at P30. Immunostaining for βgal (red) and Cux1 (green) demonstrates overlap of the two labels in neurons in layers II-IV. **(C)** High magnification of the upper-layer region of the cortical wall as stained in **(B)** shows expression of βgal (red) exclusively in Cux1-positive neurons (green). **(D)** High magnification of the lower-layer region of the cortical wall as stained in **(B)** demonstrates that the scattered βgal (red) labeling in deep layers is confined primarily to Gad65/67-positive interneurons (green). I, layer I; II/III, layers II-III; IV, layer IV; V, layer V; VI, layer VI; WM, white matter. Scale bars represent 1000 μm **(B)** and 50 μm **(C-D)**.

SUPPLEMENTAL EXPERIMENTAL PROCEDURES

Generation of mice. Gene-targeting was carried out using homologous recombination in embryonic stem cells. A *Dab1* gene-targeting vector was designed to insert LoxP sites flanking exon 2 of the *Dab1* gene, followed by a neomycin-resistance cassette (*PGK-neo*) flanked by two FRT sites. The vector was electroporated into 129P2/OlaHsd-derived E14TG2a embryonic stem (ES) cells and targeted ES cell clones were screened by PCR for targeting of the 3' arm (SP1: 5'-CTCTGGGGTTCGAATAAAG-3'; SP2: 5'-CATACGCTTGTGGTCCTATAC-3'). Positive clones were subsequently analyzed by Southern blot to confirm recombination of the 5' and 3' arms and to detect the presence of the 5' LoxP site (using HindIII digest of ES cell genomic DNA and the outside probes shown in Figure S1A). 2 confirmed clones were injected into C57BL/6J blastocysts and the resulting chimeras were then mated to C57BL/6J females to obtain germ-line transmission. Heterozygous F1 mice ($Dab1^{flox\text{-}neo/+}$) were mated with *B6.Cg-Tg(ACTFLPe)* mice (The Jackson Laboratory, Stock # 005703) to remove the *PGK-neo* cassette and the resulting offspring were subsequently mated to C57BL/6J mice to remove the *FLPe* transgene. Crossing heterozygous mice generated $Dab1^{flox/flox}$ mice and genotyping was performed by PCR (GP1: 5'-GGTTCAGTGCCTATCATGTATC-3'; GP2: 5'-GAGCCAGTGAGCGGTTCC-3') on tail DNA. $Dab1^{flox/flox}$ mice were mated to *Nestin-CRE* transgenic mice (Graus-Porta et al., 2001) and *Nex-CRE* mice (Belvindrah et al., 2007; Goebbels et al., 2006), which were genotyped as previously described (Goebbels et al., 2006; Graus-Porta et al., 2001). Double

heterozygous *Dab1*$^{flox/+}$*; Nestin-CRE* and *Dab1*$^{flox/+}$*; Nex-CRE* mice were crossed with homozygous *Dab1*$^{flox/flox}$ mice to obtain animals used in experiments.

The Cux2 gene-targeting vector was designed to insert the gene encoding CRE recombinase (CRE) into the endogenous translation start site in exon 4 of the *Cux2* gene. A PGK-neo cassette flanked by two FRT sites was included for negative selection. Gene targeting was performed at InGenious Targeting Laboratory, Inc. (Stony Brook, NY) by electroporation into C57BL/6-derived ES cells. Clones were screened by PCR for targeting of the 5' arm (SP3: 5'-AGAAGTCTCGGGGAAGCGTAAC-3'; SP4: 5'-ACCATTTCCGGTTATTCAACTT-3'). Positive clones were subsequently analyzed by Southern blot to confirm recombination of the 5' and 3' arms (using HindIII or BamHI digests of ES cell genomic DNA and the outside probes shown in Figure S7A) and by PCR (Cre1: 5'-GACATGTTCAGGGATCGCCAGGCG-3'; Cre2: 5'-GACGGAAATCCATCGCTCGACCAG-3') to confirm the presence of the CRE gene. 2 confirmed clones were injected into C57BL/6J-Tyr c-2J blastocysts and the resulting chimeras were then mated to C57BL/6J-Tyr c-2J females to obtain germ-line transmission. Breeding of F1 and F2 progeny was performed as described above and offspring were genotyped with primers Cre1 and Cre2. *Cux2*$^{cre/+}$ mice were mated to *Dab1*$^{flox/flox}$ mice to generate double heterozygous *Dab1*$^{flox/+}$*;Cux2* $^{CRE/+}$ mice, which were then crossed to *Dab1*$^{flox/flox}$ mice to obtain animals used in experiments. For staging of mice, midday of the day of the vaginal plug was considered as E0.5 and the day of birth was termed P0.

Expression Constructs. A segment of the mouse genomic region containing a promoter fragment from the *Dcx* gene was amplified by PCR (Dcx1: 5'-GTGCCACTTTTCAATTCCAGCCTTCAT-3'; Dcx2: 5'-AGTAACGGTCCCCATTGCGGTAGAA-3') and cloned as a BglII-XbaI fragment into pBluescriptII-SK+. A subfragment (SpeI-PflMI) was then cloned into a vector containing an internal ribosome entry site (IRES) and EGFP. Coding sequences for the following genes were inserted between the Dcx promoter and IRES-EGFP: NLS-CRE (Lewandoski et al., 1997), LIMK1-D460N (Edwards and Gill, 1999), Cofilin-S3A (Nagaoka et al., 1996), Akt1-K179M (Addgene plasmid 16243) (Franke et al., 1995) Rap1GAP (Han et al., 2006), Cdh2, DN-Cadherin (cytoplasmic domain of classical cadherins). Oligonucleotides containing the HA-tag sequence were ordered and cloned into pcDNA3 to create pcDNA-HA. Rap1a was amplified by PCR from E15.5 mouse brain cDNA (Rap1a-Hind-F 5'-CGTAAGCTTAGAGCGCATCATGCGTGAGTACAAG-3'; Rap1aEcoRV-R 5'-ATCCGATATCGAGCAGCAAACATGATTTCTTTTTAG-3') and cloned into pcDNA-HA. Rap1a shRNA expression vectors were purchased from Open Biosystems (TRCN0000055268 and TRCN0000055272). Cdh2 shRNAs (target sequences 5'-GACGGTCACTGCCATTGAT-3' and 5'-GCAAATCTATTTACTTGAT-3') were synthesized as oligonucleotides and cloned into a U6 promoter-containing vector.

Histology, Immunostaining and Immunoblotting. Nissl staining, immunohistological analysis and immunoblotting were performed essentially as

described (Belvindrah et al., 2007). Sections used for immunostaining were first subjected to antigen retrieval by boiling in citrate buffer. Antibodies used for immunostaining were as follows: anti-200kD Neurofilament Heavy (Smi-32) mouse monoclonal (1:2000; Abcam), anti-Chondroitin Sulfate (CS-56) mouse monoclonal (1:100; Sigma), anti-Ctip2 (25B6) rat monoclonal (1:500; Abcam), anti-Cux1 CDP (M-222) rabbit polyclonal (1:200; Santa Cruz Biotechnology), anti-Dab1 B3 rabbit polyclonal (1:400; kindly provided by J. Cooper, Fred Hutchinson Cancer Research Center), anti-FoxP2 rabbit polyclonal (1:500; Abcam), anti-GAD65/67 (1:1000; Sigma), anti-GM130 mouse monoclonal (1:250; BD Transduction Laboratories), anti-Map2 rabbit polyclonal (1:2000, kindly provided by S. Halpain, University of California – San Diego), anti-Tbr1 rabbit polyclonal (1:500; Abcam), anti-βgal (1:1000; Promega), anti-pan Cadherin (1:200; Abcam). Nuclei were stained with ToPro3 (1:10,000; Molecular Probes) and sections were mounted on slides with Prolong Gold mounting medium (Molecular Probes). Images were captured using a Fluoview FV500 (Olympus) laser-scanning confocal microscope. Image analysis and quantification was performed using MetaMorph software (Molecular Devices).

For immunoblotting from tissue, one hemisphere of the neocortex was dissected from each embryo at E16.5 and snap-frozen on liquid N_2. Tissue was then homogenized in lysis buffer (50mM Tris-HCl pH 7.6, 500 mM NaCl, 0.1% SDS, 0.5% DOC, 1% Triton X-100, 0.5 mM $MgCl_2$, with Complete Protease Inhibitor Cocktail Tablets [Roche]) on ice for 10 minutes and clarified by centrifugation at

4°C for 25 minutes. Protein concentration was determined by BCA assay (Pierce) and 75 μg of total protein was loaded for each sample. Anti-Dab1 rabbit polyclonal antibody (1:1000; Chemicon) was used for immunoblotting.

For Cdh2 Western blot, primary cortical neurons were nucleofected (Lonza AG) with Cdh2 shRNAs or control shRNA and lysed after 48 hours. For each sample, 40 μg of total protein was loaded. Anti-Cdh2 rat monoclonal antibody was used for immunoblotting (1:500; clone MNCD2 developed by M. Takeichi and H. Matsunami, obtained from the Developmental Studies Hybridoma Bank developed under the auspices of the NICHD and maintained by The University of Iowa, Department of Biology, Iowa City, IA 52242).

For Rap1-HA Western blot, 293-T cells were transfected with Rap1a or control shRNAs and Rap1a-HA. After 48 hours, cells were lysed and 40 μg of total protein was loaded for each sample. Anti-HA rat monoclonal antibody (1:2000; Invitrogen, clone 3F10) was used for immunoblotting. Anti-α-tubulin (1:2500; Sigma) was used as a loading control.

Quantitative RT-PCR. Total RNA was isolated using the RETROScript Kit (Ambion). RNA (400 ng) was reverse transcribed to cDNA using the SuperScript III Reverse Transcriptase system (Invitrogen) and specific transcripts were quantitated by real-time PCR using Chromo4 (MJ Research), gene-specific primers, and the SYBR GREEN system (Applied Biosystems). Primer sequences

for the mouse Rap1a probe sets were: Set 1 (For – 5'-CCT ACA GAA AGC AAG TCG AGG T-3', Rev – 5'-CTG TAA ATT GCT CGG TTC CTG-3'), Set 2 (For – 5'-CAT CAT GCG TGA GTA CAA GCT A-3', Rev- 5'-TGA ACA AAC TGA ACT GTC AGA GC-3'). Relative mRNA levels for Rap1a were determined using the comparative threshold cycle method (Applied Biosystems, User Bulletin 2, 1997) and normalized to glyceraldehyde-3-phosphate dehydrogenase mRNA levels.

Electron Microscopy. Embryonic (E15.5) brains were immersion fixed in one of two fixative formulations; either 4% paraformaldehyde + 1.5% glutaraldehyde in 0.1M cacodylate buffer + 1mM $CaCl_2$ or 1% paraformaldehyde + 3% glutaraldehyde in 0.1M cacodylate buffer + 5mM $CaCl_2$. The brains were buffer washed and postfixed in 1% OsO4 in 0.1M cacodylate buffer with 0.75% potassium ferricyanide for 2 hours. Following a buffer wash, tissues were dehydrated in graded ethanol series and transitioned in propylene oxide before embedding in Embed 812 / Araldite (Electron Microscopy Sciences, Hatfield PA). Thick sections (1-2μm) were cut, mounted on glass slides and stained in toluidine blue for general assessment in the light microscope. Subsequently, 70nm thin sections were cut, mounted on copper slot grids coated with parlodion and stained with uranyl acetate and lead citrate for examination on a Philips CM100 electron microscope (FEI, Hillsbrough OR) at 80kv. Images were collected using a Megaview III ccd camera (Olympus Soft Imaging Solutions, Lakewood CO).

SUPPLEMENTAL REFERENCES

Belvindrah, R., Graus-Porta, D., Goebbels, S., Nave, K.A., and Muller, U. (2007). Beta1 integrins in radial glia but not in migrating neurons are essential for the formation of cell layers in the cerebral cortex. J Neurosci *27*, 13854-13865.

Edwards, D.C., and Gill, G.N. (1999). Structural features of LIM kinase that control effects on the actin cytoskeleton. J Biol Chem *274*, 11352-11361.

Franke, T.F., Yang, S.I., Chan, T.O., Datta, K., Kazlauskas, A., Morrison, D.K., Kaplan, D.R., and Tsichlis, P.N. (1995). The protein kinase encoded by the Akt proto-oncogene is a target of the PDGF-activated phosphatidylinositol 3-kinase. Cell *81*, 727-736.

Goebbels, S., Bormuth, I., Bode, U., Hermanson, O., Schwab, M.H., and Nave, K.A. (2006). Genetic targeting of principal neurons in neocortex and hippocampus of NEX-Cre mice. Genesis *44*, 611-621.

Graus-Porta, D., Blaess, S., Senften, M., Littlewood-Evans, A., Damsky, C., Huang, Z., Orban, P., Klein, R., Schittny, J.C., and Muller, U. (2001). Beta1-class integrins regulate the development of laminae and folia in the cerebral and cerebellar cortex. Neuron *31*, 367-379.

Han, J., Lim, C.J., Watanabe, N., Soriani, A., Ratnikov, B., Calderwood, D.A., Puzon-McLaughlin, W., Lafuente, E.M., Boussiotis, V.A., Shattil, S.J.*, et al.* (2006). Reconstructing and deconstructing agonist-induced activation of integrin alphaIIbbeta3. Curr Biol *16*, 1796-1806.

Lewandoski, M., Meyers, E.N., and Martin, G.R. (1997). Analysis of Fgf8 gene function in vertebrate development. Cold Spring Harb Symp Quant Biol *62*, 159-168.

Nagaoka, R., Abe, H., and Obinata, T. (1996). Site-directed mutagenesis of the phosphorylation site of cofilin: its role in cofilin-actin interaction and cytoplasmic localization. Cell Motil Cytoskeleton *35*, 200-209.